STRESS CORROSION CRACKING OF A 52M WELD OVERLAY IN A PWR ENVIRONMENT[1,2]

Bogdan Alexandreanu, Yiren Chen, Ken Natesan and Bill Shack

Argonne National Laboratory
Argonne, IL 60439 USA

June 2015

[1]To be presented at the 17th International Conference on Environmental Degradation of Materials in Nuclear Power Systems – Water Reactors, August 9-13, 2015, Ottawa, Ontario, Canada

[2]Work supported by the Office of Nuclear Regulatory Research, U.S. Nuclear Regulatory Commission, under Job Code V-6279. The views expressed in this paper are those of the authors, not necessarily those of the U.S. Nuclear Regulatory Commission.

STRESS CORROSION CRACKING OF A 52M WELD OVERLAY IN A PWR ENVIRONMENT

Bogdan Alexandreanu, Yiren Chen, Ken Natesan, and Bill Shack

Argonne National Laboratory, Nuclear Engineering Division,

9700 S. Cass Avenue, Argonne IL 60439, USA

ABSTRACT

Weld overlays (WOL) of alloys believed to possess superior stress corrosion cracking (SCC) resistance due to their higher Cr content are typically applied over welds made with SCC-susceptible alloys with the expectation that they will act as a barrier to SCC. The objective of this work was to investigate the SCC behavior near or at the WOL interface. For this purpose, a 52M WOL was deposited on a double-J Alloy 182 weld using prototypical welding parameters. In the first set stage of this work, cracks were initiated in Alloy 182 and allowed to propagate in a direction perpendicular to the Alloy 52M WOL interface. Two identical tests conducted in this manner revealed that the average SCC propagation rates in Alloy 182 decreased by an order of magnitude to approx. 10^{-11} m/s by the time they reached the Alloy 52M interface, and that they continued to propagate past the interface into Alloy 52M at a similar reduced rate. The post-test examination found that significant crack branching occurred at the interface between the two alloys, with SCC propagation along both the original direction into Alloy 52M and the interface between the two welds. Growth along the interface between the two welds was severe, with rates estimated at approx. 10^{-10} m/s. While the average rate of propagation in Alloy 52M was measured to be in the 10^{-11} m/s range, the maximum SCC penetration into Alloy 52M was 2.5 mm which translates into an estimated maximum SCC rate an order of magnitude higher. Hence, in the second stage of this work – and this is the focus of this paper, confirmatory tests were conducted with the specimens aligned along the WOL interface. These tests substantiated the earlier findings: the SCC rate under constant load conditions at the interface between the two welds (20% Cr) was slightly faster than that in Alloy 52M near the interface (25% Cr), and both were in the 10^{-10} m/s range.

Keywords: Stress Corrosion Cracking, Alloy 52M, Weld overlay

1. INTRODUCTION

Weld overlays (WOL) of alloys believed to possess superior stress corrosion cracking (SCC) resistance due to their higher Cr content are typically applied over welds made with SCC-susceptible alloys with the expectation that they will act as a barrier to SCC. In order to test this hypothesis, an Alloy 52M WOL was fabricated at Argonne National Laboratory (ANL) Central Shops and SCC crack growth rate (CGR) testing was conducted in TS orientation on two specimens (Fig. 1) with the purpose of observing the behavior of the SCC cracks propagating from Alloy 182 into the Alloy 52M WOL.[1] In both tests the known fatigue, corrosion fatigue, and SCC behavior of Alloy 182 was reproduced early, and it was concluded that both cyclic and SCC CGRs in Alloy 182 are un-affected by the Alloy 52M WOL at distances larger than 1-1.5 mm from the WOL interface. However, in tests of this type, the exact location of the crack was essential, hence, once the cracks approached the interface, loading had always had to include a cyclic component to minimize the effect of unbroken ligaments. The approach resulted in controlled, uniform crack fronts starting approx. 1 mm ahead of the Alloy 52M interface in both cases. The SCC CGRs in Alloy 182 were found to decrease by approx. one order of magnitude in the 1 mm leading up to the interface; also, the environmental enhancement of the cyclic rates mirrored this behavior, hence, it substantiated the decreasing trend of the SCC CGRs. In addition, the behavior of cyclic rates near the interface was a critical piece of information for the management of one subsequent test in the ST orientation – and this will be described later in this paper.

Both tests in the TS orientation have shown that the SCC behavior at the Alloy 182-52M interface is complex. On the one hand, cracking along the interface, in a direction normal to the original direction of propagation (i.e., ST) was severe (Fig. 2). On the other hand, cracking was found to propagate directly (along the initial plane of propagation, TS) in a finger-like manner – consistent with SCC - into Alloy 52M. Specifically, SCC cracking was found to penetrate into Alloy 52M over 40% of interface, and in one instance, cracking was observed to extend for 2.5 mm into Alloy 52M (Fig. 3), yielding a maximum SCC CGR of 2×10^{-10} m/s (a conservative estimate for K in this case is 34 MPa $m^{1/2}$).

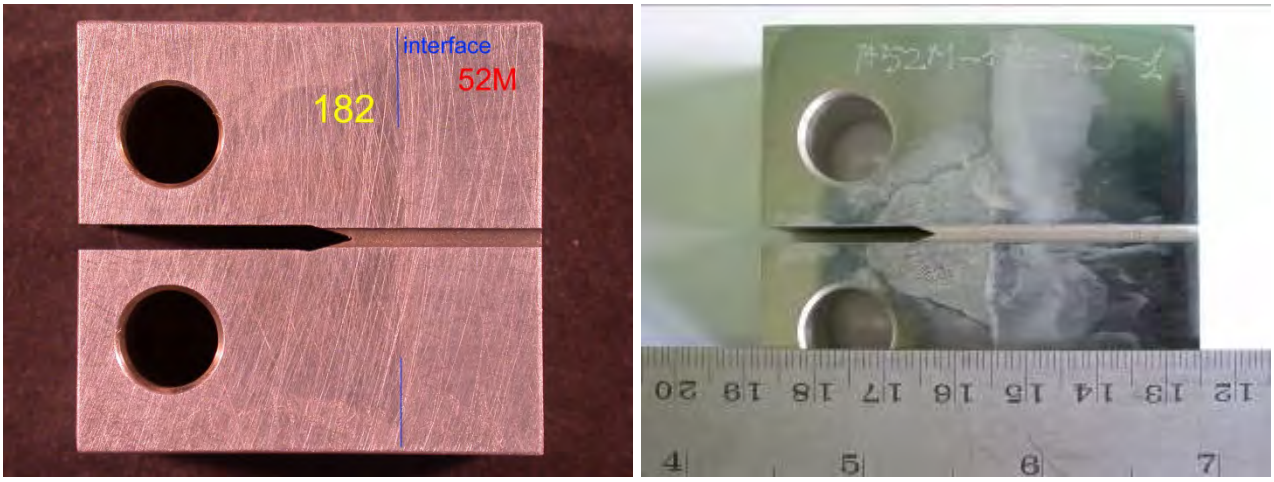

(a) (b)

Figure 1. Photographs of the Alloy 52M-182 WOL specimens tested in the TS orientation.

(a) (b)

Figure 2. Fractured specimens (a) A52M-182-TS-3, and (b) A52M-182-TS-1. Note the severity of cracking along the interface and into Alloy 52M.

(a)

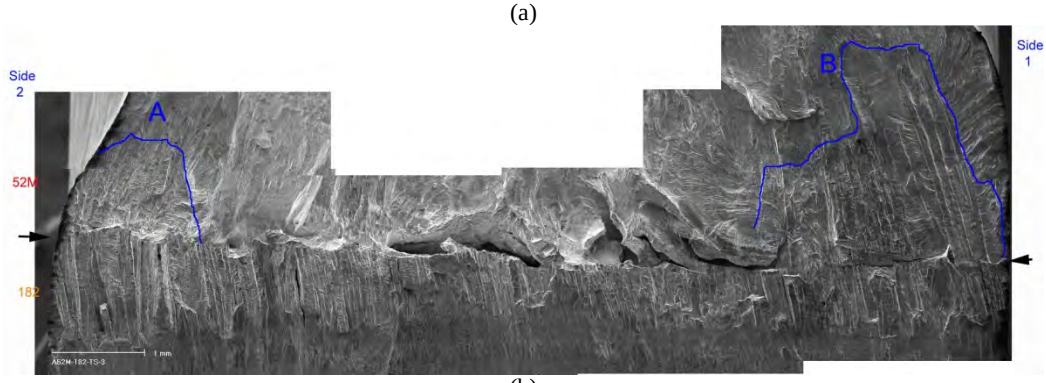

(b)

Figure 3. Fracture surface of Specimen A52M-182-TS-3: (a) photograph, and (b) SEM micrograph. The maximum crack length in area B is 2.5 mm, yielding an estimated maximum SCC CGR of $2x10^{-10}$ m/s. The black arrows indicate the interface between the two welds. Crack propagation is from bottom to top.

In summary, severe cracking was observed along the interface between the two welds as well as in Alloy 52M near the interface in the TS-oriented specimens. As such, SCC CGR testing was next undertaken along those planes with the objective of measuring the SCC CGRs directly. This paper presents two tests conducted on specimens in the ST orientation (Fig. 4). In both specimens, the test plane was tilted approx. 15º with respect to the Alloy 52M-182 interface. In one case, the crack is growing from Alloy 182 towards the interface with Alloy 52M. In the second case, the crack is initiated in Alloy 52M and grows towards the interface with Alloy 182.

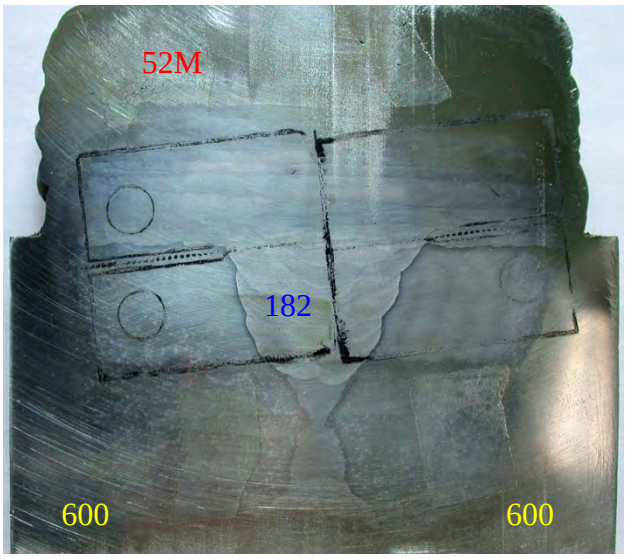

Figure 4. (a) Specimens for SCC CGR testing of Alloy 52M-182 WOL in the ST orientation.

2. EXPERIMENT

This section describes the WOL fabrication, test specimens, and the CGR test apparatus and experimental approach.

2.1 Alloy 52M WOL

The Alloy 52M (Heat NX75W1TK) weld overlay (Fig. 5) was deposited on top of an existing Alloy 182 weld. The Cr concentrations for the two alloys were 29.98% and 14.35%, respectively. The Alloy 182 weld had been tested previously (without the overlay), and a set of both cyclic and SCC CGR data existed for this weld.

The Alloy 52M WOL was produced at ANL Central Shops using prototypical welding parameters. The Alloy 52M deposit was made with 1/8"-dia. wire, current 158-160A, voltage 16V, travel speed 3.5-4 in./min, 99.99% Ar shield gas 22-26 CFH, oscillation approx. 1/4, weave approx. 1/4. The bead was 0.562" wide, and the crown height above base metal was 1/16".

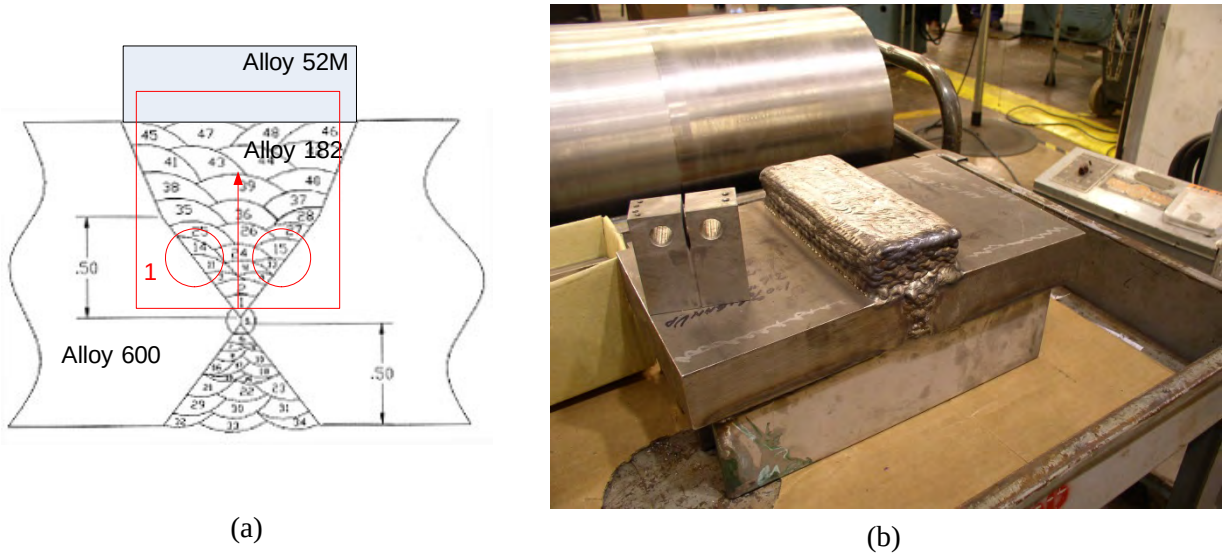

(a) (b)

Figure 5. (a) Conceptual schematic, and (b) photograph of the resulting Alloy 52M-182 weld overlay. The continuous welded restraints used during the Alloy 52M WOL deposition are visible in the photograph.

2.2 SCC CGR testing

The SCC CGR testing conducted in test facility with SS autoclaves configured for CT specimens. A detailed description of these facilities is provided elsewhere.[2-3] Crack extensions were determined by the reversing-DC-potential-drop technique. The simulated PWR feed water contained 2 ppm Li, 1000 ppm B, ≈2 ppm dissolved hydrogen (≈23 cm^3/kg), and less than 10 ppb dissolved oxygen (DO). The water was recirculated through the autoclave at a rate 50 ml/min. The test temperature was 320°C.

3. RESULTS

As a result of the severe cracking observed along the interface between the two welds as well as in Alloy 52M near the interface in the TS-oriented specimens, SCC CGR testing was next undertaken along those SCC-susceptible planes. As such, two tests were conducted on specimens in the ST orientation (Fig. 4). In both ST specimens, the test plane was tilted approx. 15° with respect to the interface.

3.1 SCC along the Alloy 52M-182 interface, Specimen WOL-ST-1

The objective of this test was to measure the SCC CGR along the interface between the Alloy 52M WOL and Alloy 182. In this specimen (Fig. 6), the crack was initiated in Alloy 600, was expected to reach the Alloy 182 weld after approx. 1 mm, and then was advanced in Alloy 182 until it reached the Alloy 52M/182 interface. At that point, the specimen was set at constant load to measure the SCC CGR along the interface. The fatigue behaviors of Alloys 600 and 182 are well-known, and were used to manage the test. The testing conditions and CGR responses are given in Table 1.

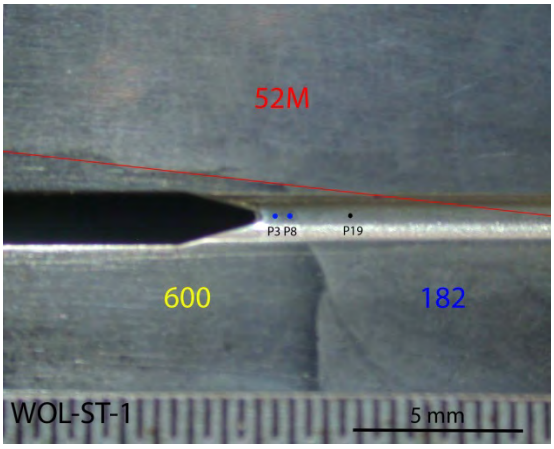

Figure 6. Notch area in specimen WOL-ST-1. The red line shows the Alloy 52M WOL interface.

The specific configuration of Specimen WOL-ST-1 (Fig. 6) also offered an opportunity to assess the cyclic and SCC behavior in Alloy 600 HAZ from the Alloy 182 weld. As such, two sets of cyclic and SCC measurements were conducted in the Alloy 600 HAZ. The SCC CGR was first evaluated in test period 3 at approx. 0.7-0.65 mm from the Alloy 182 weld interface. Next, the crack was advanced for approx. 0.45 mm, and the SCC CGR was evaluated again in a region 0.2-0.1 mm from the interface in test period 8.

Figure 7 summarizes the cyclic and SCC CGRs measured in the Alloy 600 HAZ region of specimen WOL-ST-1. Figure 7a shows the measured cyclic CGR data vs. the expected CGRs in air under the same loading conditions, and for comparison, the expected curves in air and environment for Alloy 600 (blue) and Ni-base weld (green) are included in the figure. As expected, the cyclic CGRs measured in this stage of the test are consistent with the known response of Alloy 600. The data obtained prior to the first test period at constant load (3, dark blue symbols) seem lower than the data obtained prior to the second test period at constant load (8, light blue symbols). The comparison shown in Fig. 7a seems to suggest that the cyclic CGRs of the HAZ increase as the crack approaches the Alloy 182 weld interface. Figure 7b shows the SCC CGRs measured for Alloy 600 HAZ in test periods 3 (dark blue symbol) and 8 (light blue

symbol), and these also increase as the crack approaches the fusion line. As such, Fig. 7 suggests that both cyclic and SCC CGRs appear to increase as the crack advances towards the interface. However, Fig. 7b also includes a "reference" SCC CGR obtained from the same heat of Alloy 600 (NX 131031), tested in the same ST orientation separately. The similarity in responses between the "reference" and test period 3 (approx. 0.6 mm from the fusion line) suggests that in this case, the HAZ does not extend more than approx. 0.6 mm from the fusion line, and the effect on the SCC CGR response was approx. a factor 2.

Table 1. Crack growth data for specimen WOL-ST-1 in PWR water[a].

Test Period	Test Time, h	Temp. °C	Load Ratio R	Rise Time, s	Down Time, s	Hold Time, s	K_{max}, MPa·m$^{1/2}$	ΔK, MPa·m$^{1/2}$	CGR_{env}, m/s	Estimated CGR_{air}, m/s	Crack Length, mm
Pre a	173	321.6	0.30	1	1		24.8	17.4	7.15E-09	2.05E-08	12.015
Pre b	189	321.6	0.30	50	50		24.9	17.4	4.98E-10	4.15E-10	12.028
Pre c	193	321.6	0.30	0.5	0.5		25.3	17.7	1.77E-08	4.47E-08	12.163
Pre d	196	321.6	0.30	1	1		25.5	17.8	1.28E-08	2.30E-08	12.218
Pre e	213	321.6	0.30	50	50		25.6	17.9	7.77E-10	4.66E-10	12.242
1	237	321.7	0.50	50	12		25.7	12.8	2.56E-10	2.04E-10	12.271
2	263	321.7	0.50	300	12		25.6	12.8	9.24E-11	3.37E-11	12.275
3	406	321.7	1.00	0	0		25.7	0.0	7.93E-11	-	12.312
4	408	321.9	0.20	0.5	0.5		26.5	21.2	5.31E-08	7.45E-08	12.495
5	411	321.7	0.20	0.5	0.5		24.6	19.7	5.72E-08	5.47E-08	12.704
6	429	321.7	0.50	50	12		24.8	12.4	3.89E-10	1.78E-10	12.771
7	433	321.8	0.50	300	12		24.8	12.4	2.04E-10	2.98E-11	12.779
8	668	321.6	1.00	0	0		25.2	0.0	1.63E-10	-	12.885
9	671	321.6	0.20	0.5	0.5		26.8	21.4	5.29E-08	7.76E-08	13.345
10	676	321.6	0.20	0.5	0.5		23.0	18.4	2.01E-08	1.27E-07	13.451
11	692	321.6	0.20	50	50		23.0	18.4	1.41E-09	1.28E-09	13.464
12	701	321.8	0.20	1	1		23.2	18.6	3.40E-10	6.69E-08	13.528
13	717	321.6	0.20	50	50		23.3	18.6	1.00E-09	1.34E-09	13.528
14	724	321.7	0.20	0.5	0.5		23.8	19.1	1.64E-08	1.49E-07	13.719
15	741	321.6	0.20	50	50		24.0	19.2	2.38E-09	1.53E-09	13.770
16	748	321.7	0.20	0.5	0.5		25.0	20.0	7.73E-08	1.79E-07	14.013
17	764	321.7	0.50	50	12		26.3	13.2	9.22E-10	6.98E-10	14.379
18	837	321.7	0.50	300	12		26.7	13.4	2.68E-10	1.24E-10	14.446
19	6,472	321.3	1.00	0	0		46.6	0.0	1.30E-10	-	17.265

[a]Simulated PWR water with 2 ppm Li, 1000 ppm B, and 2 ppm. DO<10 ppb. Conductivity was 21±3 μS/cm, and pH 6.4.

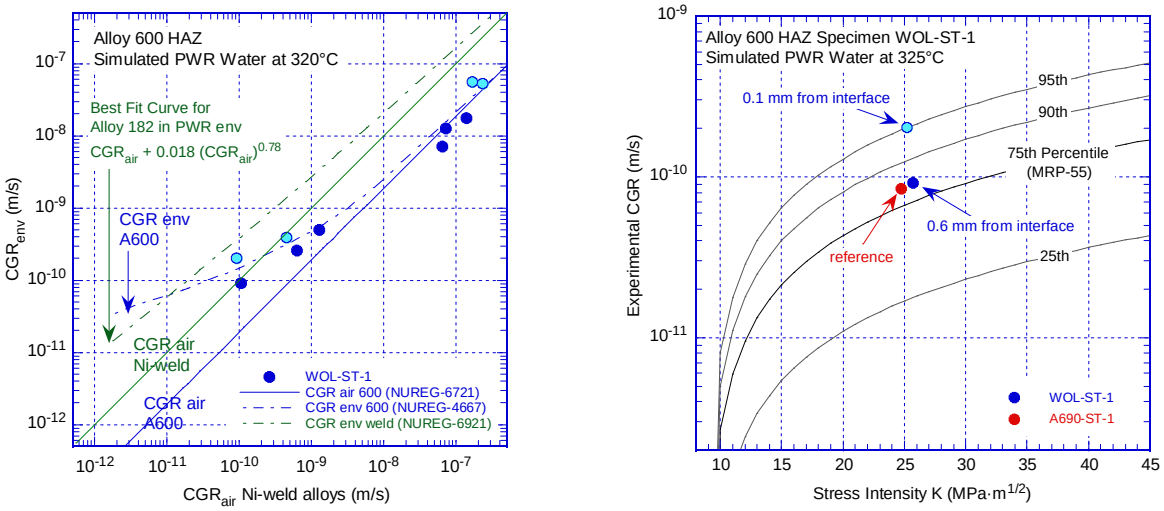

Figure 7. (a) Cyclic CGR data for the Alloy 600 (HAZ) region of specimen WOL-ST-1 in simulated PWR environment; (b) SCC CGR data for the Alloy 600 (HAZ) region of specimen WOL-ST-1 and MRP-55 disposition curve for Alloy 600.[4]

Next, the crack was advanced in fatigue across the Alloy 600-182 interface into Alloy 182, and Fig. 8 shows the cyclic response in Alloy 182. For comparison, the expected curves in air and environment and for Alloy 600 (blue) and Ni-base weld (green) are included in the figure. The response seems lower than expected for a Ni-base weld, and this was interpreted as an off-plane advance. As such, it was assessed that the crack turned towards the interface with Alloy 52, hence, the specimen was set at constant load in what was estimated to be the vicinity of the Alloy 52M-182 interface in test period 19.

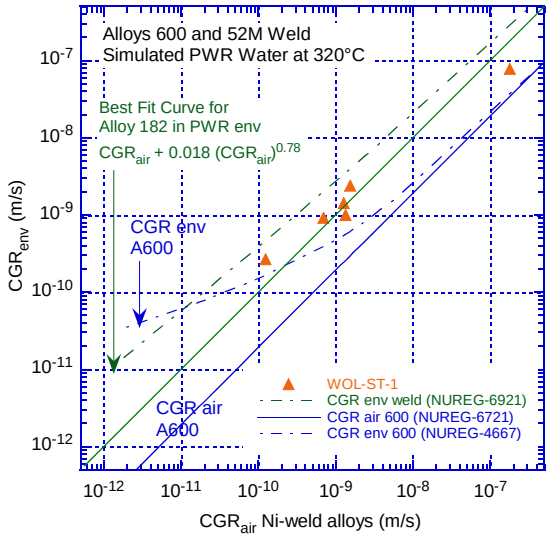

Figure 8. Cyclic CGR data for the Alloy 182 region of specimen WOL-ST-1 in simulated PWR environment.

Figure 9 shows the SCC response of the Alloy 182-Alloy 52M interface (the data was corrected based on the fractographic information which will be presented later in this section). The initial SCC CGR of $2.8x10^{-10}$ m/s (up to approx. 1240h) was unexpectedly high given the orientation of the crack front with respect to the dendrites, then began to diminish and continued at the diminished rate of approx. $1.3x0^{-10}$ m/s for the remainder of the test. Also, small "jumps" have been observed and these are indicated by arrows in the figure. It was verified that these jumps are neither the result of some errant loading nor an electrical artifact. In fact, they are regions of fast growth (10^{-8} m/s) that occurs over short periods of time (15-20 min). The cause of the "jumps" is unknown, however, as it will be shown later in this paper, they are a signature of SCC along the interface between these two welds.

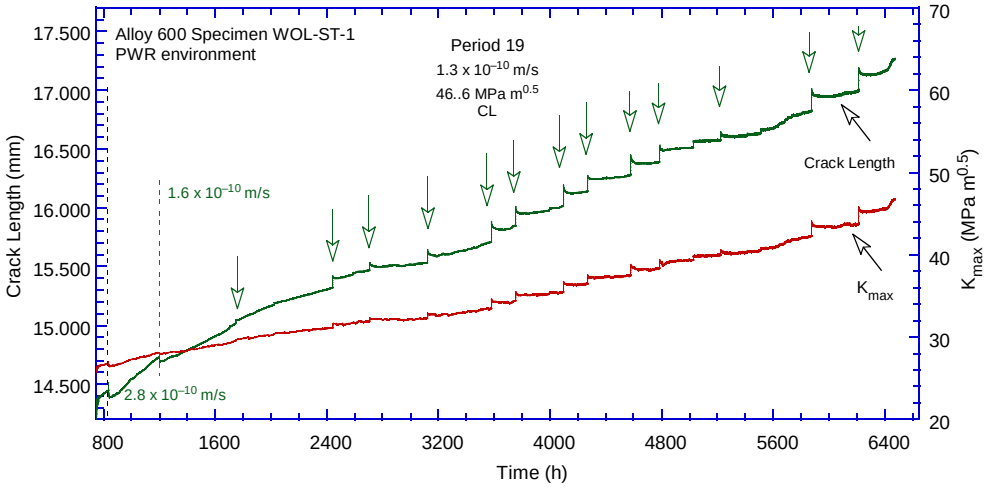

Figure 9. Crack–length–vs.–time for specimen WOL-ST-1 in simulated PWR environment during test period 19. The data were corrected by a factor 8.2 following the analysis of the fracture surface.

The post test-examination of this specimen involved both the side surfaces and that of the fracture surface.

In order to show the side cross sections, the side surfaces were ground to eliminate the side grooves, polished and electrochemically etched in a 5% nital solution. The two side surfaces (Fig. 10) show that the test progressed largely as anticipated during the test (Fig. 6), and confirm that cracking initiated in Alloy 600, transitioned into Alloy 182 weld, and then along the Alloy 182/52M interface.

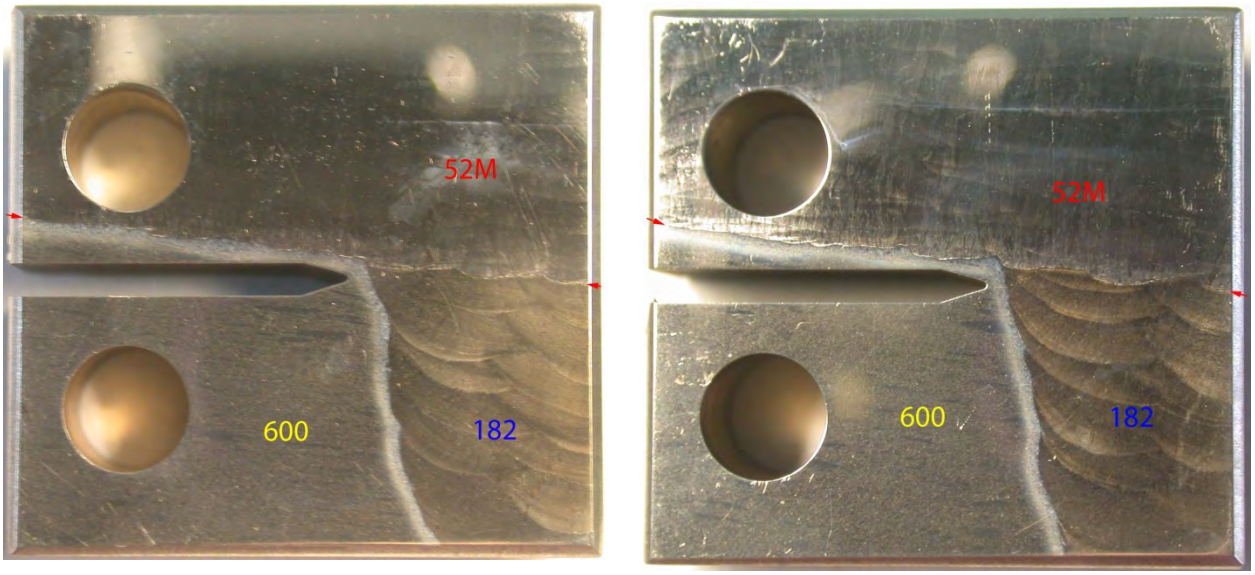

(a) (b)

Figure 10 Post-test specimen WOL-ST-1 seen from both sides: (a) side 1, and (b) side 2. The red arrows indicate the Alloy 52M WOL interface. Crack advance is from left to right.

The two side surfaces were further examined by optical microscopy, Fig. 11. The blue arrows indicate the Alloy 600/182 interface, and the red arrows indicate the Alloy 182-52M interface. Both cross sections show that after passing through the Alloy 600-182 interface, the crack turns towards the Alloy 52M WOL interface. This off-plane cracking caused the Alloy 182 cyclic data appear less than expected, Fig. 8. The two cross sections show that the crack was driven in the vicinity of the Alloy 182-52M WOL as anticipated: on one surface (side 1), the crack under cyclic loading overshoots slightly the WOL interface, while on the second surface (side 2), the crack ends up slightly below the interface. Overall, the two images shown in Fig. 11 demonstrate that the specimen was set at constant load in the vicinity of the Alloy 182-52M WOL interface, and, hence, test period 19 represents cracking along the interface.

Figure 12 provides additional detail on the crack path. Figure 12a was taken at location 1B in Fig. 11a, at the end of the test. EDS analysis shows that the preferred crack path was through a region with an average Cr concentration of 18%. Figure 12b was taken at location 2B in Fig. 11b, and the EDS analysis shows that the preferred crack path was through a region with an average Cr concentration of 18-20%. In summary, EDS analysis shows that in this test, cracking occurred preferentially along the Alloy 182-52M WOL interface with Cr concentrations of 18-20%.

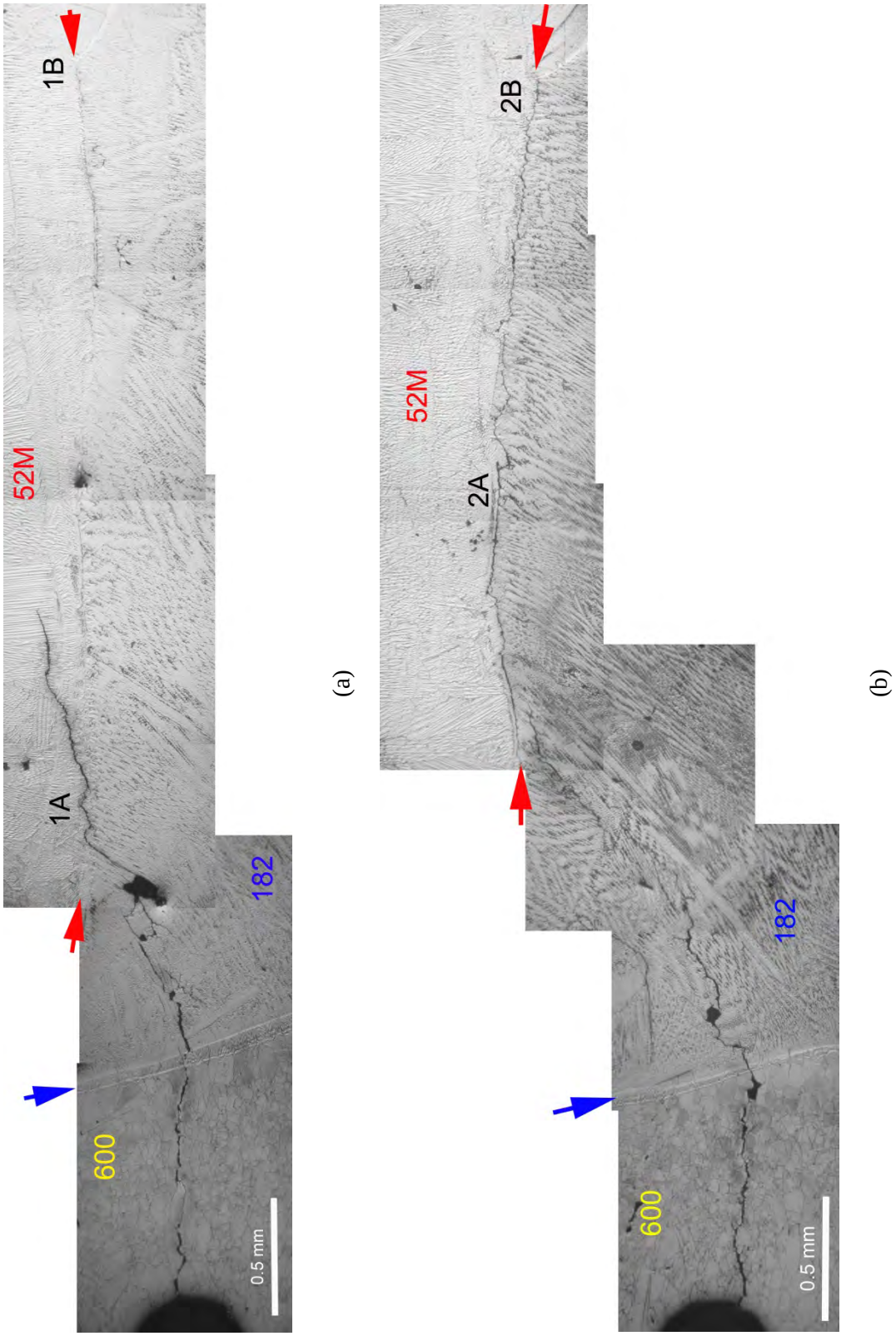

Figure 11. Cross sections of specimen WOL-ST-1: (a) side 1, and (b) side 2. Blue arrows indicate the Alloy 600/182 interface and the red arrows indicate the Alloy 182/52M interface. Crack advance is from left to right.

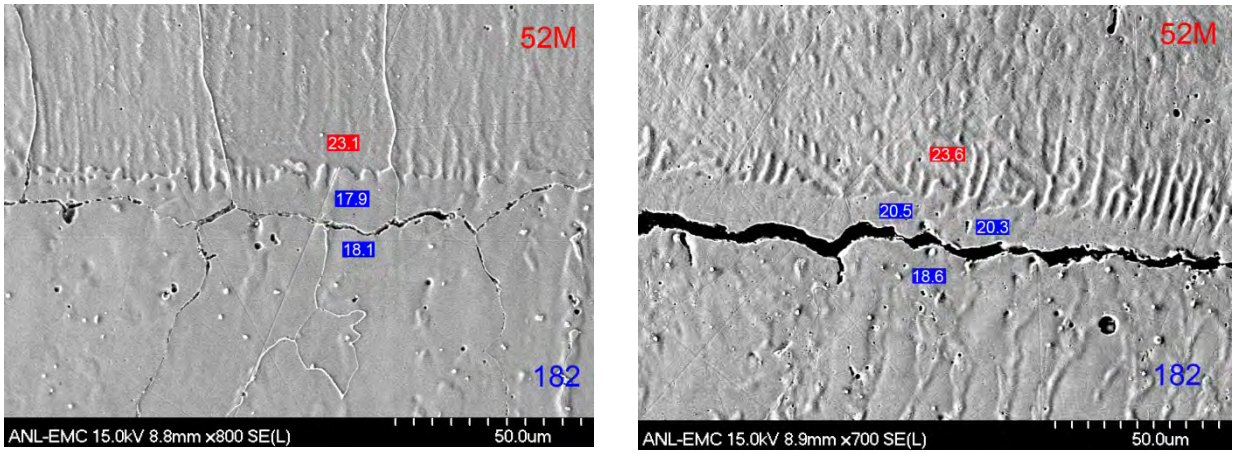

(a) (b)

Figure 12 Micrographs on the cross section of specimen WOL-ST-1 on (a) side 1 taken at location 1B in Fig. 11a, and (b) side 2 taken at location 2B in Fig. 11b. Inserts show the local Cr concentrations (wt. %). Crack advance is from left to right.

Following the examination of the side surfaces, the specimen was fatigued in air at room temperature to break some of the remaining ligaments, and was fractured after cooling in liquid nitrogen. The fracture surface was photographed (Fig. 13) and was examined in the SEM (Fig. 14).

The photograph, Fig. 13, provides a good visual contrast between the various alloys that were tested. Blue arrows indicate the Alloy 600-Alloy 182 interface, green arrows indicate the Alloy 182-Alloy 52M interface, and the red arrows and line mark the end of the test. The locations of the two test periods in Alloy 600 (P3 and P8) and along the Alloy 52M-182 interface (P19) are indicated in the figure. Measurements show that the Alloy 600-182 interface is 1.06 mm from the notch, in good agreement (5%) with expectations. The crack reaches the Alloy 52M-Alloy 182 interface after 2.61 mm, again in good agreement (2%) with the distance measured by DC potential through test period 18, Table 1, which was 2.54 mm. The end of the test is 5.50 mm from the specimen notch, hence, the crack extension under constant load in test period 19 is 2.89 mm, a factor of 8.2 higher than the 0.339 mm extension measured by DC potential. The final crack extension was re-measured on the SEM image (Fig. 14) and was found to be in very good agreement (7%) with the determination based on Fig. 13. As such, test period 19 was corrected by a factor 8.2, and the outcome is shown in Fig. 9. Table 1 already reflects the corrected rate.

The SEM examination also allowed for a closer inspection of the fracture features. Several areas of interest are marked in Fig. 14, and will be presented next.

Figures 15 is an image taken at location 2 in Fig. 14, and focuses on the Alloy 182-Alloy 52M transition. The blue arrows indicate the onset of cracking in Alloy 182, and the image seems to show that occasional TG fracture (white arrows) occurred prior to transitioning into Alloy 52M. These regions correspond to location 1A in Fig. 11a where the crack under fatigue loading slightly overshot the Alloy 52M WOL interface. Nevertheless, the crack seems to have eventually transitioned to IG, and one of the early occurrences is indicated with a green arrow.

Figure 16 shows images taken at locations 4, 5 in Fig. 14, and illustrate the fracture mode obtained under constant load in this specimen. Out-of-plane cracking was observed at several locations but this did not appear to be a predominant feature. The lack of out-of-plane cracking suggests that the interface was indeed the most susceptible microstructure for crack propagation. Overall, the aspect of the fracture mode was as expected, i.e., with the dendrites normal to the plane of the figure.

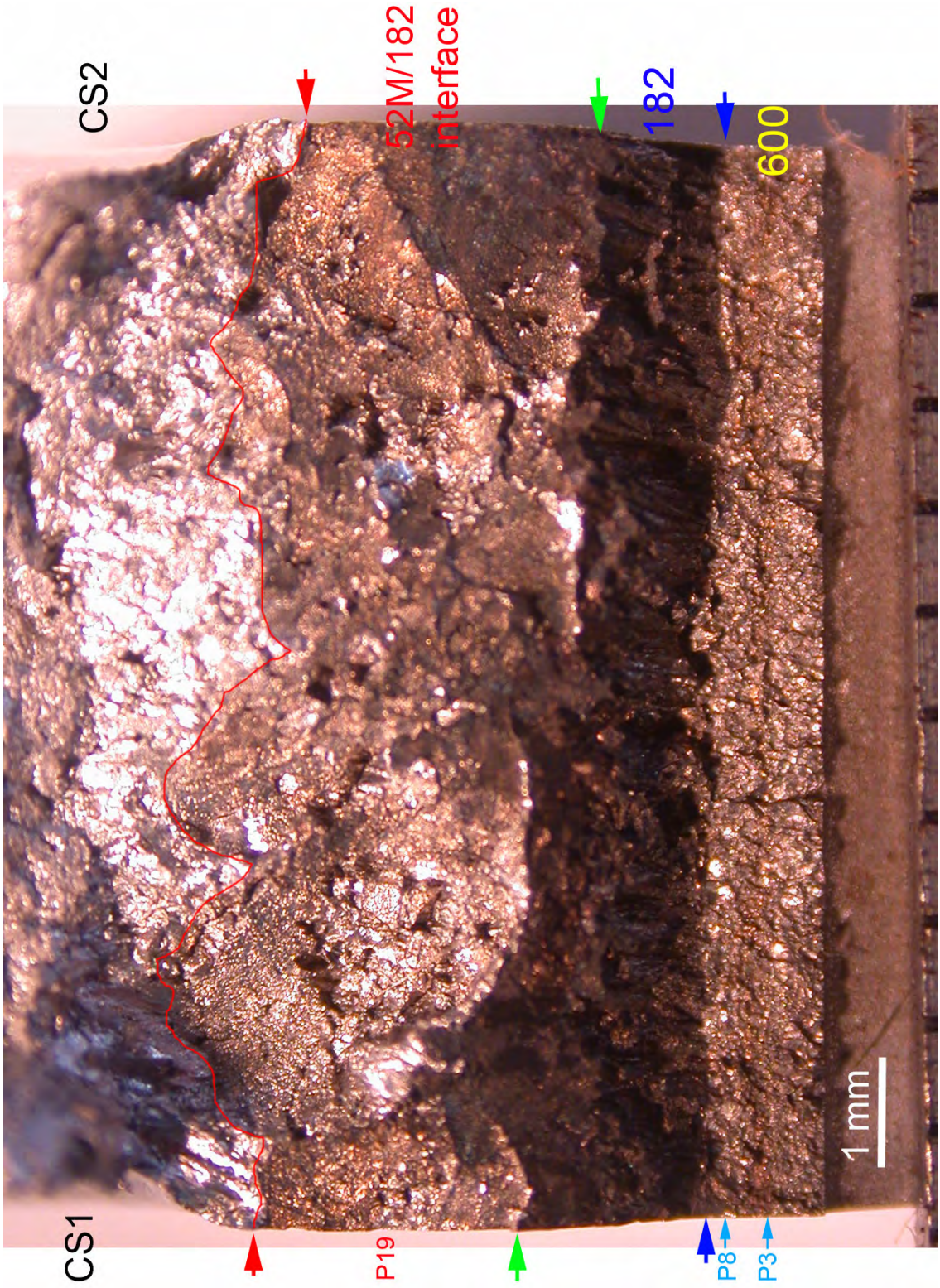

Figure 13. Fracture surface of specimen WOL-ST-1. The blue arrows indicate the Alloy 600-182 interface, the green arrows indicate the Alloy 182-52M interface, and the red arrows indicate the end of the test. The approximate locations of select test periods P3, P8 and P 19 are indicated in the figure. Crack advance is from bottom to top.

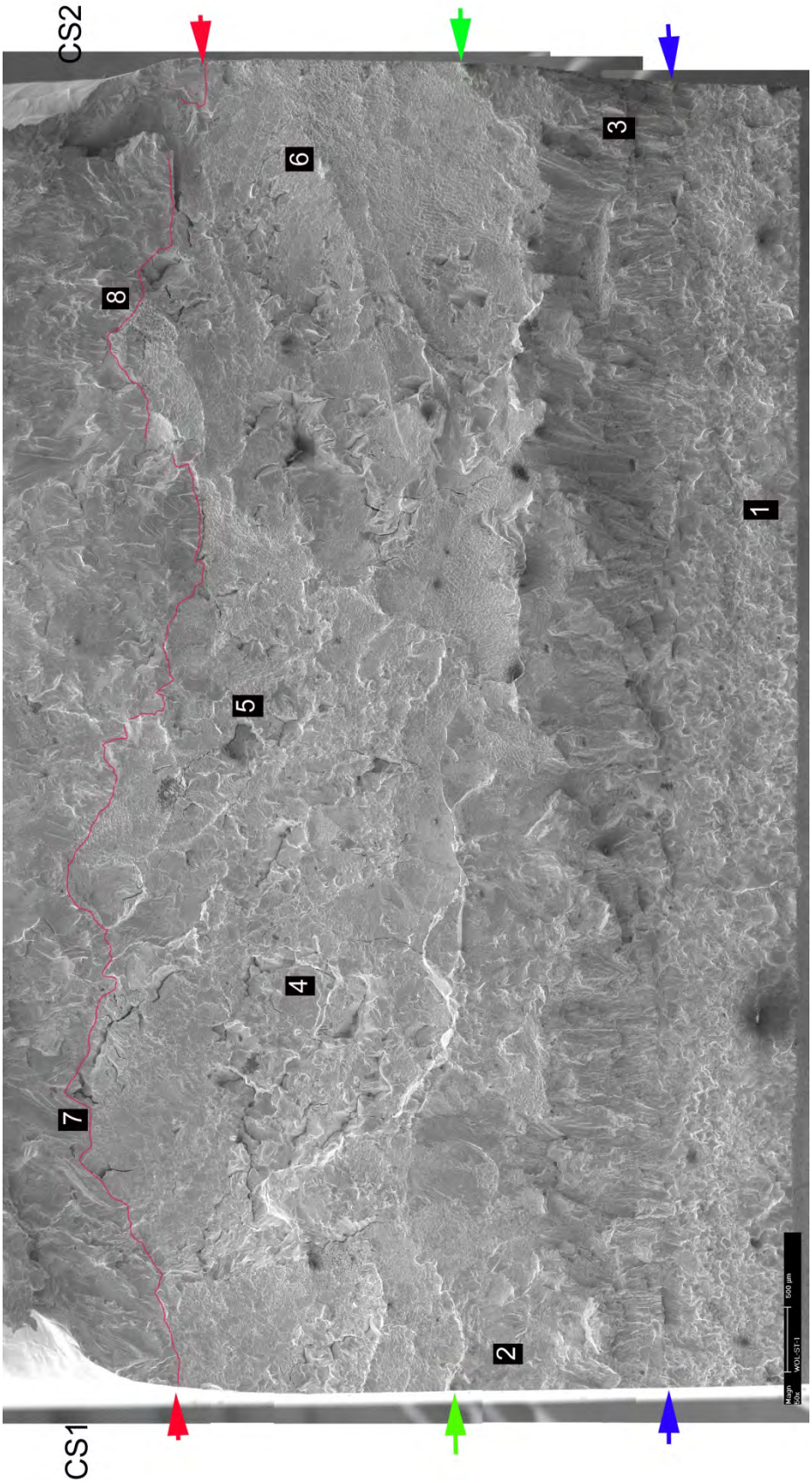

Figure 14. Fracture surface of specimen WOL-ST-1. The blue arrow indicates the Alloy 600-182 interface, the green arrow indicates the Alloy 182-52M interface, and the red arrow indicates the end of the test. Crack advance is from bottom to top.

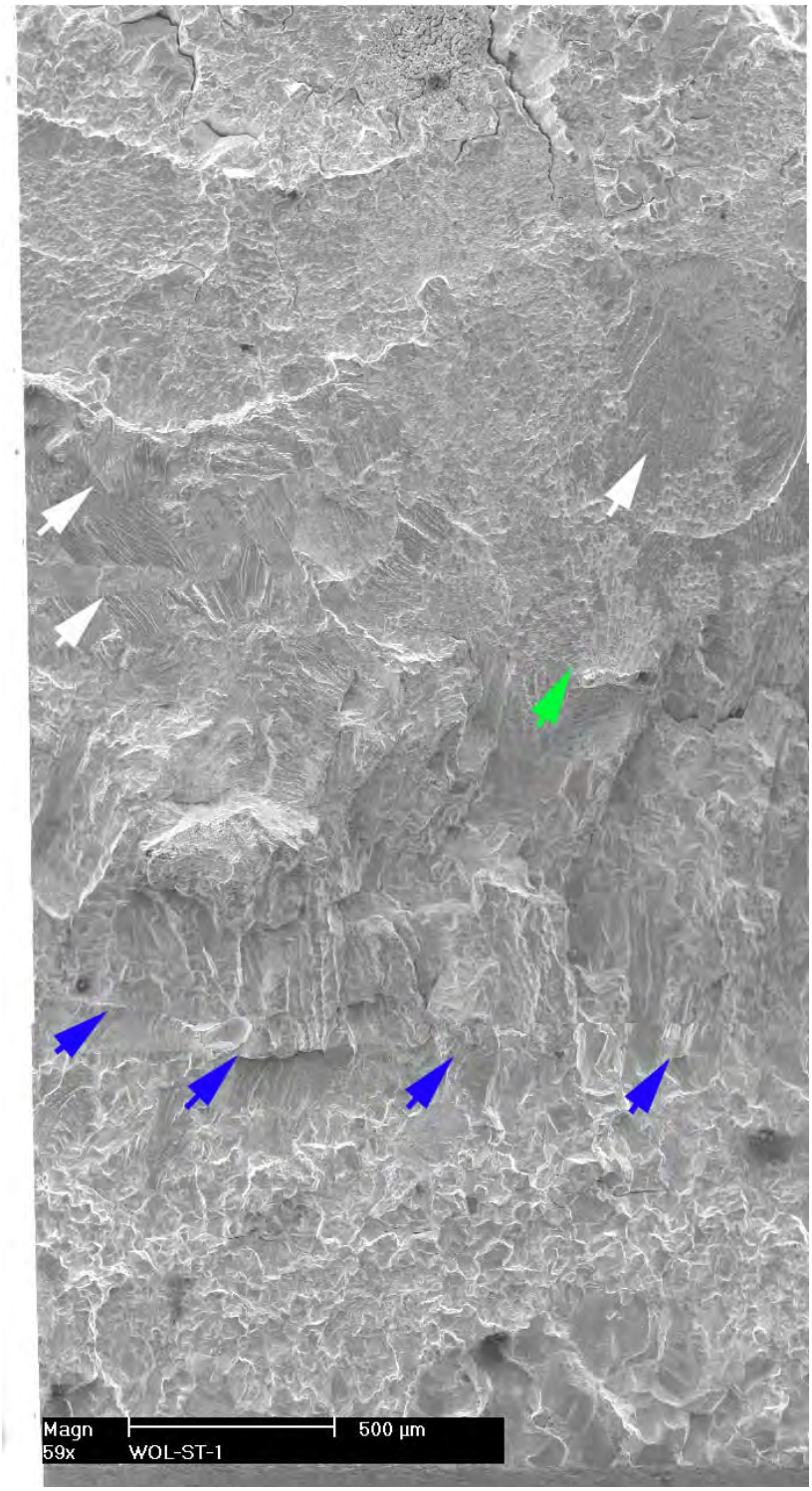

Figure 15 Fracture surface of specimen WOL-ST-1 at location 2 in Fig. 14. The blue arrows indicate the onset of cracking in Alloy 182, and white arrows indicate the occasional TG fracture that occurred prior to transitioning into Alloy 52M. These regions correspond to location 1A in Fig. 11a where the crack under fatigue loading overshot the WOL interface. The green arrow indicates a region with IG features. Crack advance is from bottom to top.

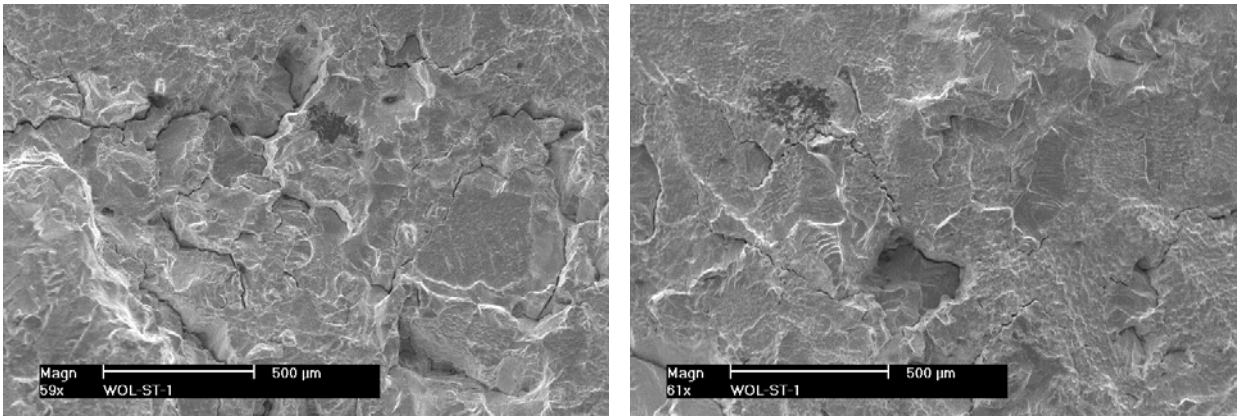

(a) (b)

Figure 16 Fracture surface of specimen WOL-ST-1 at (a) location 4, and (b) location 5 in Fig. 14. Crack advance is from bottom to top.

3.2 SCC along the in Alloy 52M near the interface with Alloy 182, Specimen WOL-ST-2

The objective of the test on Specimen WOL-ST-2 was to measure the SCC CGR in Alloy 52M near the interface with Alloy 182. In this specimen the crack was initiated in Alloy 52M and was expected to reach the Alloy 182 weld after approx. 6 mm of growth, Fig. 17. Based on prior observations (Fig. 3), the expectation for this test was for the crack to find a highly SCC-susceptible region in Alloy 52M near the interface, then continue on the interface between the two welds as the prior WOL-ST-1 test showed that that is the most susceptible path; moreover, prior testing[1] showed that Alloy 182 near the WOL was relatively resistant.

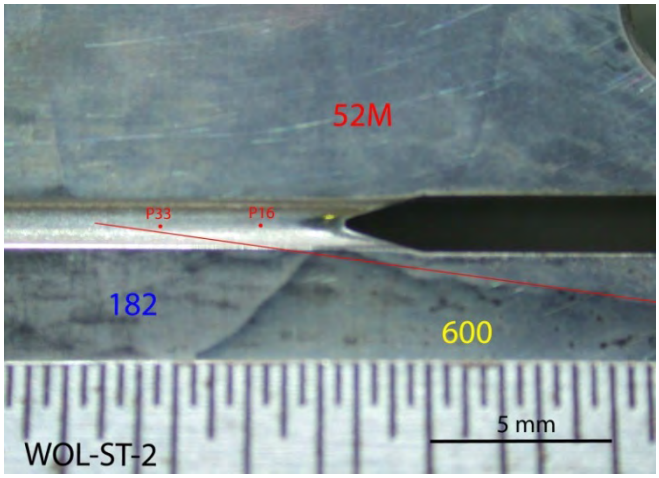

Figure 17. Notch area in specimen WOL-ST-2. The red line shows the Alloy 52M WOL interface.

The testing conditions and CGR responses are given in Table 2. The test was initiated with precracking in the PWR environment (as usual), and this was followed by transitioning steps, and the known[5,6] fatigue and corrosion fatigue behavior for the Ni-base weld were reproduced (Fig. 18). Early attempts at measuring an SCC CGR yielded very low rates (10^{-12} m/s), and it is not clear whether the unfavorable orientation with respect to the dendritic grains played a role or not. Nevertheless, regions of high SCC susceptibility were known to exist from the earlier TS tests (Fig. 3), hence it was decided to advance the crack while closely monitoring the environmental enhancement of the cyclic rates. This was accomplished in test periods 20-31. Figure 19 tracks the environmental enhancement of two loading conditions – rise 50s and rise 600s, R = 0.5 – vs. crack advance from the notch (propagation is from right to left to match Fig. 17). The purpose of the fast cycle is to advance the crack, and the purpose of the slow cycle is to probe for environmental enhancement. The dotted red and blue horizontal lines represent

the environmental enhancement levels of a forward advancing crack based on the Alloy 152 experience.[7] In those tests - conducted at ANL on an Alloy 152 weld that was produced in a symmetric, double-J geometry - it was found that environmental enhancement peaks during cyclic with load ratios of R = 0.5, and rise time of 600s, and the resulting fracture mode is IG. Based on that experience, a similar level of environmental enhancement in the current test (period 31) was interpreted as IG SCC propagation in a forward direction that can readily be measured by DC potential, and the specimen was set at constant load (test period 33). The SCC CGR response under constant load is shown in Fig. 20.

Table 2. Crack growth data for 52M specimen WOL-ST-2 in PWR water[a].

Test Period	Test Time, h	Temp. °C	Load Ratio R	Rise Time, s	Down Time, s	Hold Time, s	K_{max}, MPa·m$^{1/2}$	ΔK, MPa·m$^{1/2}$	CGR_{env}, m/s	Estimated CGR_{air}, m/s	Crack Length, mm
Pre a	196	319.5	0.31	0.5	0.5		20.0	13.8	1.20E-08	4.94E-08	11.229
Pre b	214	319.4	0.31	50	50		20.2	13.9	4.63E-10	5.12E-10	11.241
Pre c	216	319.5	0.31	0.5	0.5		20.2	14.0	1.07E-08	5.20E-08	11.260
Pre d	221	319.5	0.31	1	1		20.4	14.1	6.12E-09	2.67E-08	11.314
Pre e	237	319.5	0.31	50	50		20.4	14.1	4.52E-10	5.35E-10	11.324
Pre f	241	319.5	0.31	1	1		20.5	14.2	9.34E-09	2.76E-08	11.395
Pre g	298	319.5	0.31	100	100		20.7	14.2	3.79E-10	2.82E-10	11.432
Pre h	302	319.4	0.31	1	1		20.9	14.4	1.12E-08	2.95E-08	11.523
Pre i	416	319.1	0.31	50	50		21.1	14.6	5.67E-10	6.19E-10	11.611
Pre j	420	318.7	0.31	1	1		21.6	14.9	2.45E-08	3.36E-08	11.764
Pre k	423	318.7	0.31	2	2		21.8	15.0	1.41E-08	1.74E-08	11.828
Pre l	462	318.9	0.31	50	50		22.0	15.2	1.30E-09	7.29E-10	11.921
Pre m	467	319.3	0.31	1	1		23.2	16.0	4.07E-08	4.50E-08	12.307
Pre n	469	319.5	0.31	2	2		23.3	16.1	2.65E-08	2.33E-08	12.365
1	533	319.1	0.49	300	12		27.1	13.8	3.76E-10	1.33E-10	12.465
2	804	319.9	0.49	600	12		27.6	14.1	1.58E-10	7.28E-11	12.618
3	870	319.9	0.49	600	12	7200	27.7	14.1	2.86E-11	5.72E-12	12.621
4	999	319.1	1.00	0	0		27.7	0.0	3.69E-12		12.621
5	1,060	319.4	0.49	600	12	7200	27.6	14.1	1.95E-11	5.59E-12	12.627
6	1,099	320.2	0.49	600	12		27.1	13.8	1.05E-10	6.77E-11	12.645
7	1,516	320.2	0.49	600	12	7200	27.7	14.1	1.76E-11	5.68E-12	12.673
8	1,607	320.4	0.49	600	12		28.4	14.5	1.28E-10	8.24E-11	12.711
9	2,191	320.4	0.49	600	12	7,200	28.6	14.6	1.47E-11	6.55E-12	12.743
10	2,383	320.6	0.49	600	12		29.1	14.8	1.10E-10	9.15E-11	12.817
11	2,815	320.7	0.49	600	12	7,200	29.0	14.8	1.29E-11	6.97E-12	12.838
12	3,157	320.2	0.49	600	12		29.4	15.0	1.25E-10	9.37E-11	12.970
13	3,415	320.2	0.49	120	12		29.8	15.2	6.61E-10	5.03E-10	13.380
14	3,487	320.8	0.49	600	12		29.6	15.1	2.05E-10	9.85E-11	13.432
15	3,487	320.8	0.49	600	12	7,200	29.7	15.1	2.63E-11	7.58E-12	13.442
16	4,308	320.6	1.00	0	0		29.9	0.0	2.75E-12		13.450
17	4,408	319.9	0.49	120	12		28.8	14.7	8.14E-10	4.32E-10	13.629
18	4,477	320.0	0.49	600	12		29.3	14.9	2.18E-10	9.33E-11	13.679
19	4,992	320.6	0.49	600	12	7,200	29.5	15.0	2.33E-11	7.40E-12	13.718
20	5,051	320.1	0.49	120	12		29.3	14.9	7.31E-10	4.65E-10	13.866
21	5,214	320.3	0.44	120	12		26.4	14.8	6.39E-10	3.86E-10	14.101
22	5,285	320.4	0.42	600	12		26.2	15.2	1.87E-10	8.18E-11	14.149
23	5,454	320.4	0.43	120	12		28.4	16.2	8.39E-10	5.51E-10	14.563
24	5,549	320.1	0.49	120	12		29.2	14.9	7.70E-10	4.61E-10	14.788
25	5,617	319.9	0.49	600	12		29.4	15.0	2.28E-10	9.46E-11	14.836
26	5,687	319.7	0.49	120	12		30.7	15.7	9.11E-10	5.65E-10	15.035
27	5,806	319.6	0.47	120	12		30.5	16.1	1.10E-09	6.02E-10	15.372
28	5,977	319.9	0.48	120	12		30.8	16.0	9.49E-10	6.06E-10	15.815
29	5,996	319.9	0.48	600	12		30.8	16.0	2.68E-10	1.20E-10	15.830
30	6,144	318.9	0.50	120	12		31.3	15.7	8.81E-10	5.78E-10	16.172
31	6,210	319.6	0.50	600	12		31.4	15.7	4.38E-10	1.18E-10	16.244
32	6,282	320.4	0.50	600	12	7,200	32.8	16.4	5.32E-10	1.09E-11	16.371
33	7,867	319.2	1.00	0	0		44.2	0.0	2.97E-10	-	17.815
34	7,986	319.4	1.00	0	0		31.1	0.0	5.88E-11	-	17.818

[a]Simulated PWR water with 2 ppm Li, 1000 ppm B, and 2 ppm. DO<10 ppb. Conductivity was 21±3 μS/cm, and pH 6.4.

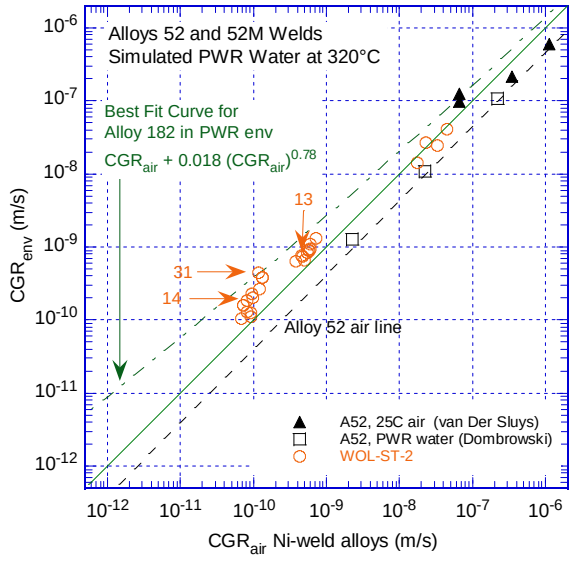

Figure 18. Cyclic CGRs for Alloy 52M specimen WOL-ST-2 in simulated PWR environment. Also included are Alloy 52 data from the literature[5,6] obtained in air at room temperature and in PWR environment.

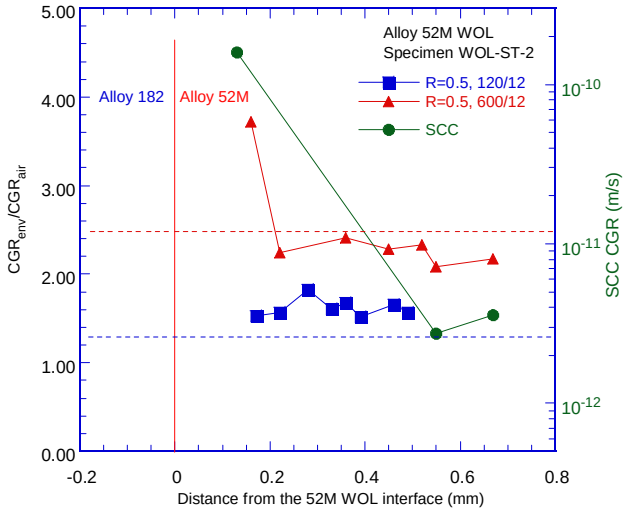

Figure 19. Environmental enhancement of two control test conditions vs. calculated distance to the interface. Crack propagation is from right to left (see also Fig. 17 for guidance)

Figure 20 shows that under constant load conditions, the initial SCC CGR of 1.6×10^{-10} m/s (K = 32.3 MPa $m^{1/2}$) was maintained until approx. 7,100h for the first 0.46 mm of growth. Next, the rate appeared to increase, and the SCC CCR was on average approx. double, 3.8×0^{-10} m/s. It is interesting to note that in the latter part of this test period (7,700 h), 5-10 µm "jumps" similar to those seen for some time in specimen WOL-ST-1 (Fig. 9) were observed; these features suggest that the crack reached the interface with Alloy 182. Finally, as the SCC CGR reached 1.4×10^{-9} m/s (after 7,855h), the specimen was unloaded. It is also interesting to note that although the unload at the end of test period 33 was intended to stop the growth (and effectively end the test), the crack continued to grow at a substantial rate even after the stress intensity factor was drastically decreased. Hence, this last period received its own designation, test period 34 in Table 2. Post-test measurements on three cross sections (the two sides of the specimen and one additional cross section in the middle of the specimen - details will be presented later in this section - confirmed that the SCC crack initiated in Alloy 52M, at least 0.8 mm from the interface with Alloy 182.

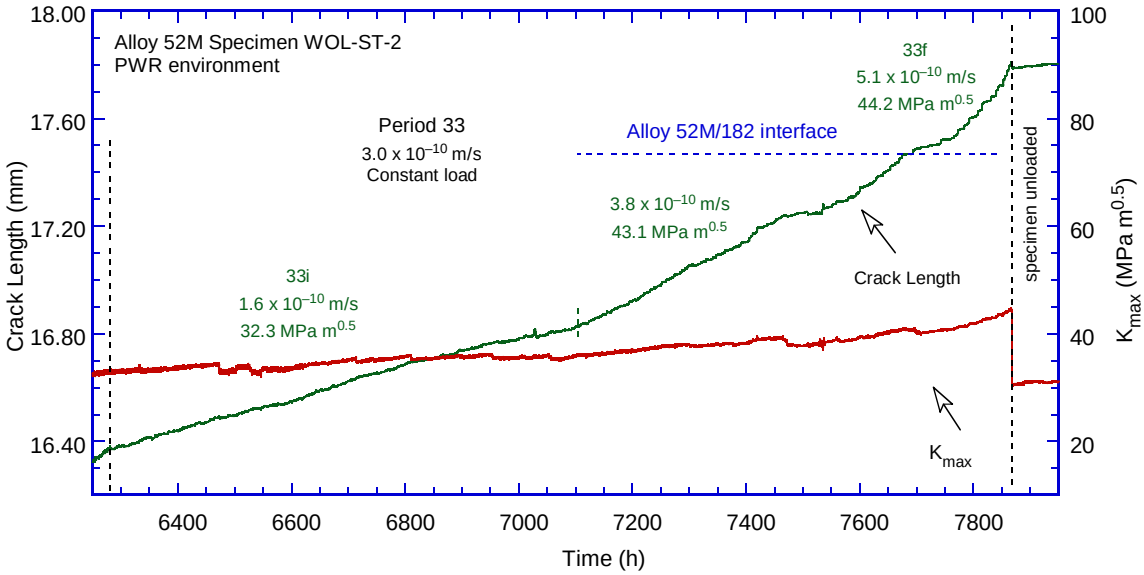

Figure 20. Crack–length–vs.–time for Alloy 52M specimen WOL-ST-2 under constant load in simulated PWR environment. The data were corrected by a factor 4.2 following the analysis of the fracture surface.

The post test-examination of this specimen involved the examination of the side surfaces (cross sections) as well as that of the fracture surface.

For this test, the examination of the side surfaces was an essential for determining the crack path. For this purpose, the side surfaces of the specimen were ground to eliminate the side grooves, polished and electrochemically etched in a 5% nital solution. The two side surfaces (Fig. 21) show that the test progressed as anticipated, and confirm that the test took place in the Alloy 52M dilution – interface area, as was intended. The distance from the specimen notch to the Alloy 182 interface measured on the two surfaces is 6.2 mm, 1% from the value estimated prior to the test (Fig. 17).

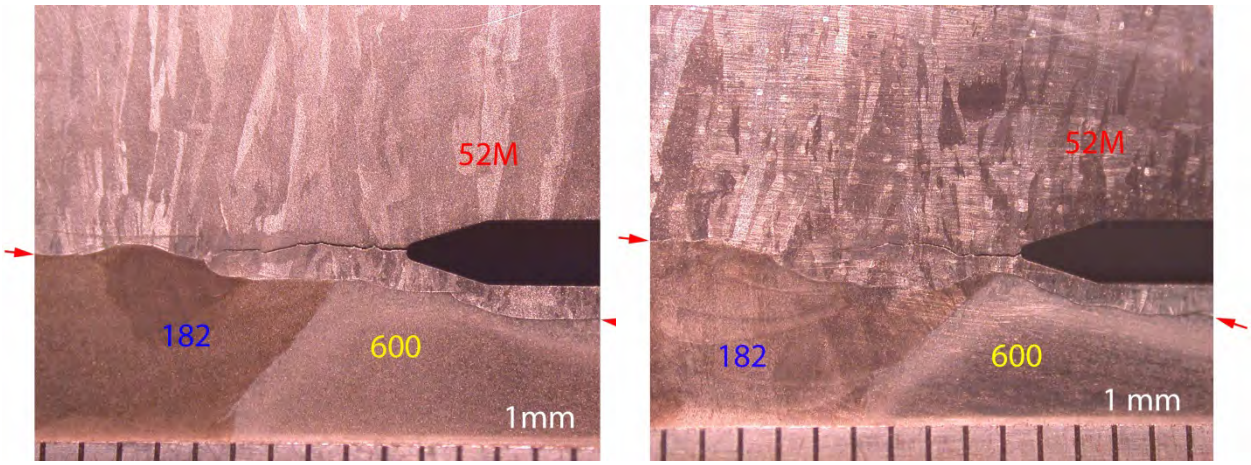

(a) (b)

Figure 21 Notch area post-test in specimen WOL-ST-2 seen from both sides: (a) side 1, and (b) side 2. The red arrows indicate the WOL interface. Crack advance is from right to left.

The two side surfaces were further examined by optical microscopy, Fig. 22. The crack advance was straight, and the large opening suggests a TG fracture mode for the most part of the test. The extent of the TG advance measured on the two side surfaces is 5.01 mm, a value which corresponds to test period 31

(Table 2). This finding suggests that the onset of high environmental enhancement in test period 31 corresponds to a change in fracture mode from TG to IG.

The IG regions initiating in the areas marked 1A and 2A in Figs. 22a and 22b, respectively, were further examined in the SEM. Figure 23 shows the IG region on side 1 of the specimen. Chemical composition measurements show that Cr levels were on average 25.5 wt. % along the IG crack path, and no Cr gradient seems present. By contrast, Cr levels at location 1B –corresponding to test period 16 with no SCC growth – were 27.1 wt. %. The figure also reveals that the IG crack appears to have taken a more SCC-susceptible direction, i.e., along the dendritic grains, towards the interface, but the clear path seems to be obstructed by a ligament. Nevertheless, cracking along the interface seems extensive, 1.6 mm from the end of the TG region. Secondary cracking in Alloy 182 is also visible.

Figure 24 shows the IG region on side 2 of the specimen (beginning at location marked 2A in Fig. 22b). Chemical composition measurements at the TG-IG transition area show that Cr levels were on average 26.6 wt. %, however, the crack did not seem to propagate much. For comparison, Cr levels at location 2B in Fig. 22b –corresponding to test period 16 with no SCC growth – were 28.1 wt. %. Nevertheless, the crack appears to have taken a more favorable direction towards the interface, and it resurfaces at the interface with Alloy 182, 0.9 mm away. As with the previous cross section, cracking along the interface seems extensive, and ends 1.2 mm from the TG region. Extensive secondary cracking in Alloy 182 is also visible.

In order to gain additional information regarding the crack propagation in the dilution zone of Alloy 52M, an additional cross section was created by sectioning the specimen in the middle. This middle cross section is shown in Fig. 25. As with the two side surfaces, the crack advance was straight with a large opening suggesting a largely TG fracture mode. Nevertheless, Fig. 25 show that following the TG growth, the crack propagated in an IG fashion towards the interface, perhaps along a more favorable weld orientation. Figure 26 (taken at location A in Fig. 25) shows that the average Cr content along the crack path was 24.2 wt. %. By contrast, Cr levels at location B in Fig. 25 –corresponding to test period 16 with no SCC growth – were on average 27.1 wt. %. As with the previous two examples, cracking along the interface seems extensive, 2.2 mm from the end of the TG region. Extensive secondary cracking in Alloy 182 is also visible.

In summary, the examination of three cross sections revealed that the test evolved as planned: the crack was transitioned to IG in the diluted area of Alloy 52M WOL, was allowed to propagate towards the interface, and towards the end of the test it reached and propagated along the interface. SCC cracking at constant load seemed to span three regions: diluted Alloy 52M WOL in the beginning, Alloy 52M/182 interface at the end, and most likely a combination of the two in the middle. This sequence seems to describe the evolution observed during test period 33 in Fig. 20.

The Cr content of the diluted Alloy 52M WOL seems to play a role: SCC occurred in regions with a Cr content which was on average 25.4 wt. %, and did not occur in regions with Cr content of 27.1 wt. %. Also, qualitatively, cracking appeared to be the most extensive in the middle cross section (24.2 wt. %), followed by side 1 (25.5 wt. %); side 2 (26.6 wt. %) showed the least amount of propagation.

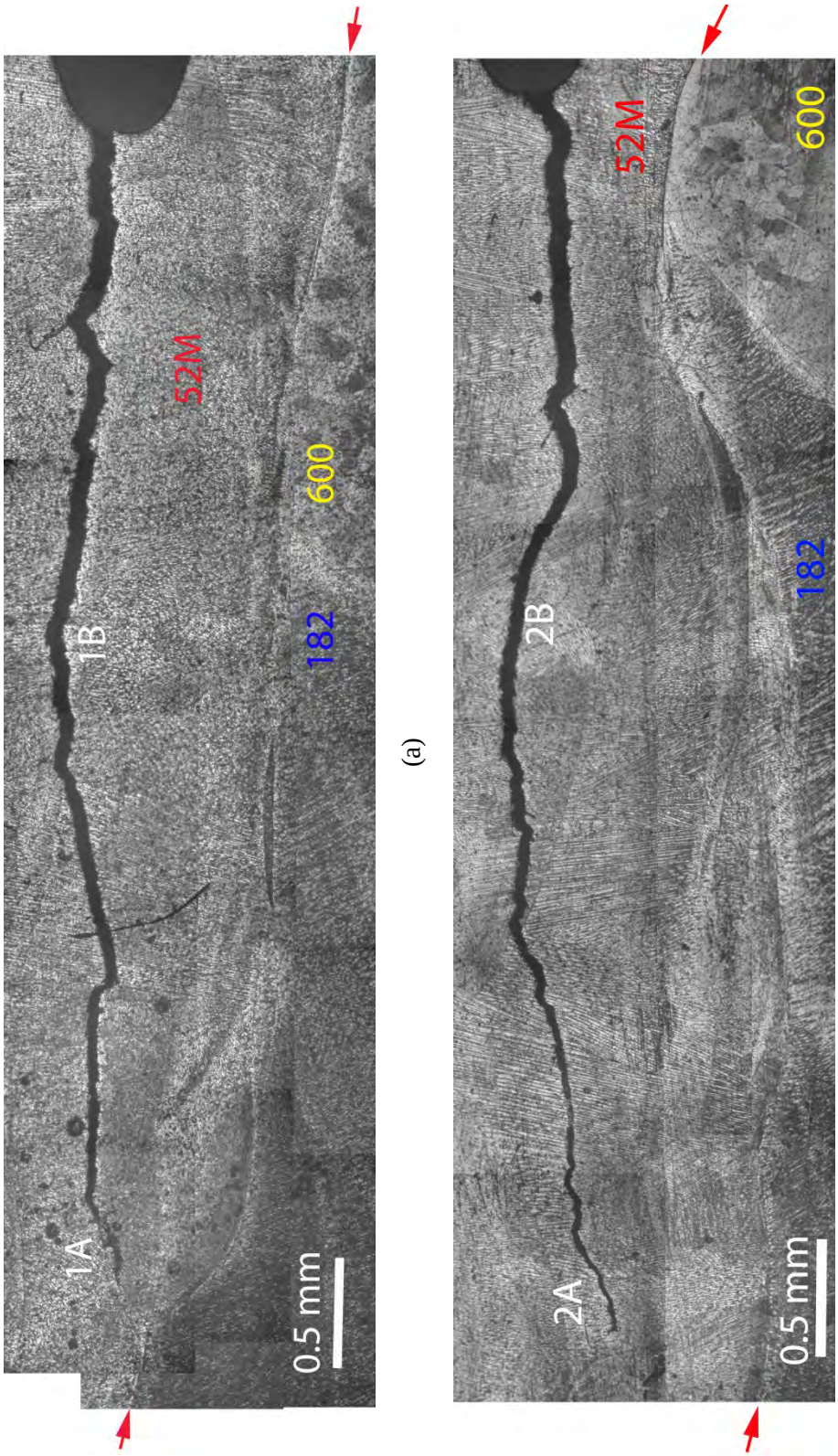

Figure 22. Cross section of specimen WOL-ST-2: (a) side 1, and (b) side 2. Crack advance is from right to left. The red arrows indicate the WOL interface.

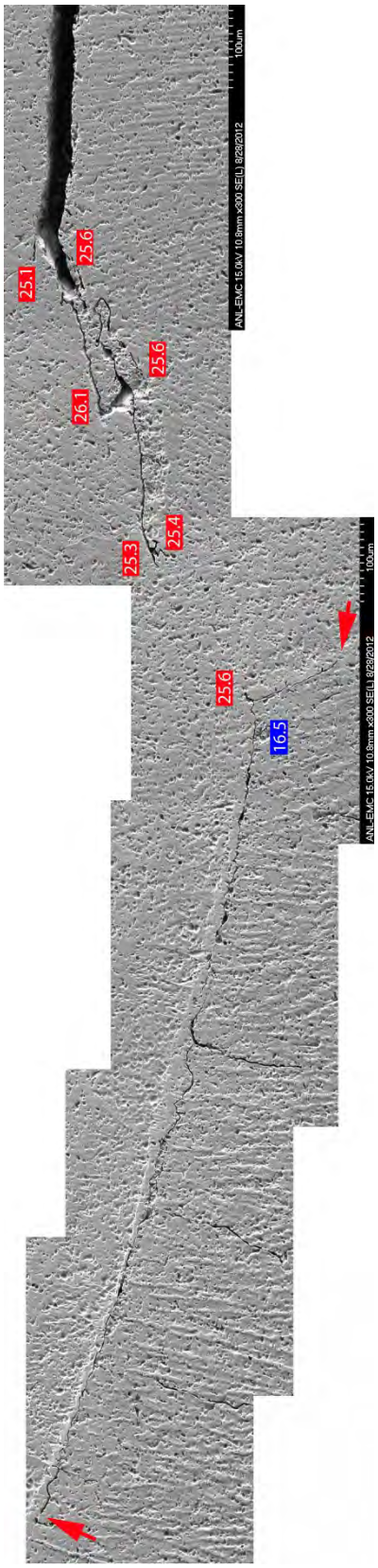

Figure 23. Crack tip region on the first side surface of specimen WOL-ST-2 (side 1, location 1A in Fig. 22a). Crack advance is from right to left. Cr concentration at select locations is indicated in the figure. The red arrows indicate the WOL interface.

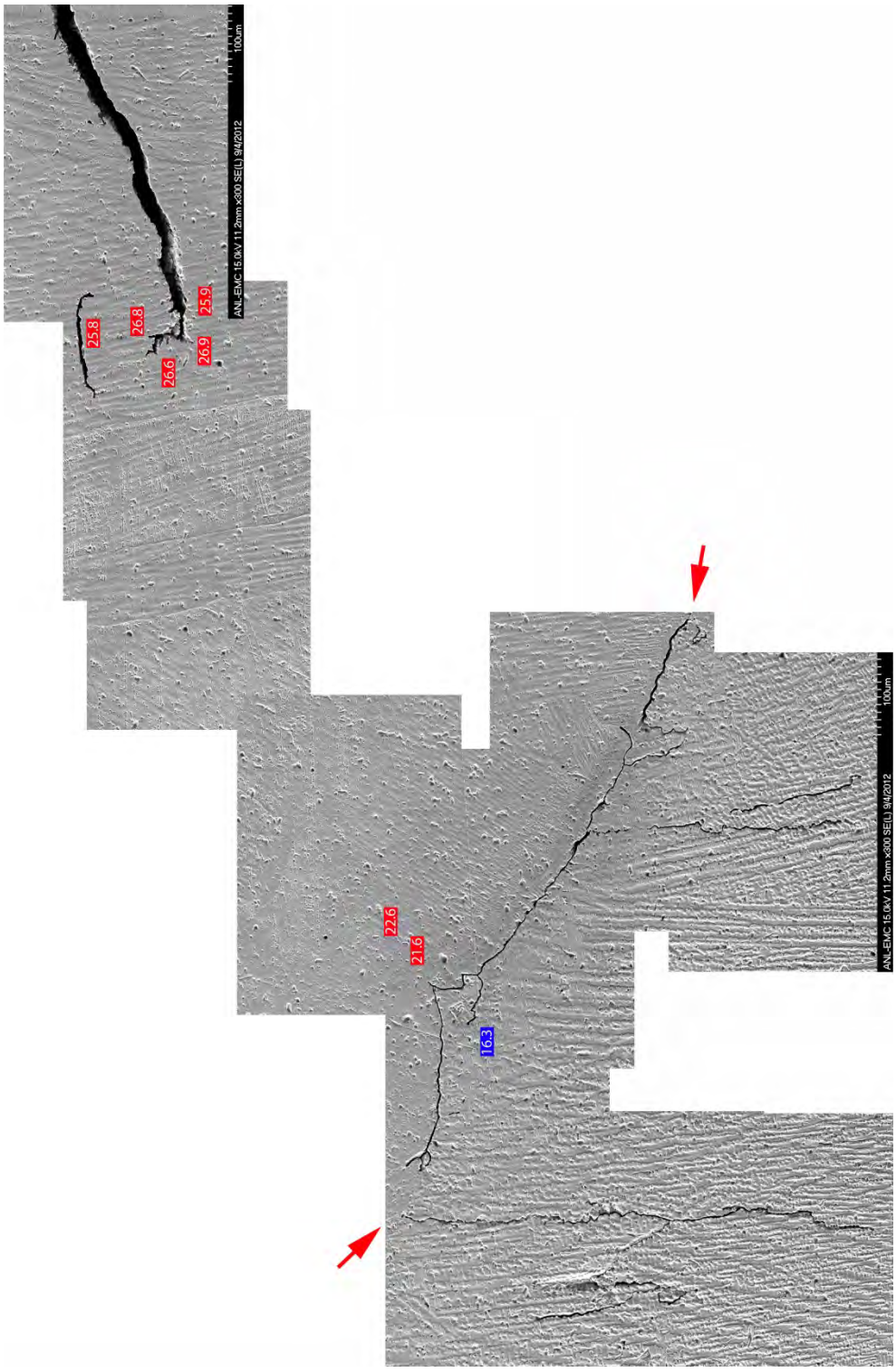

Figure 24. Crack tip regions on the second side surface of specimen WOL-ST-2 (side 2, location 2A in Fig. 22b). Crack advance is from right to left. Cr concentration at select locations is indicated in the figure. The red arrow indicates the WOL interface.

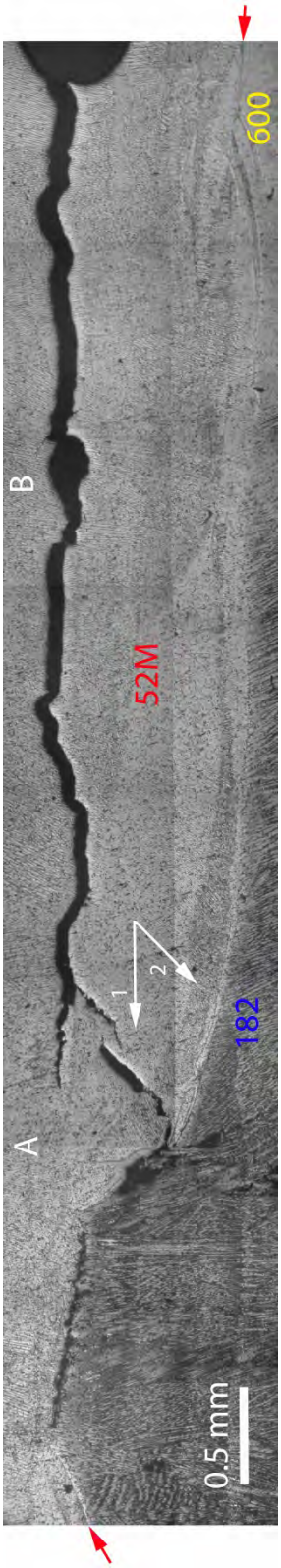

Figure 25. Cross section of specimen WOL-ST-2: taken in the middle of the specimen. Crack advance is from right to left. The red arrows indicate the WOL interface.

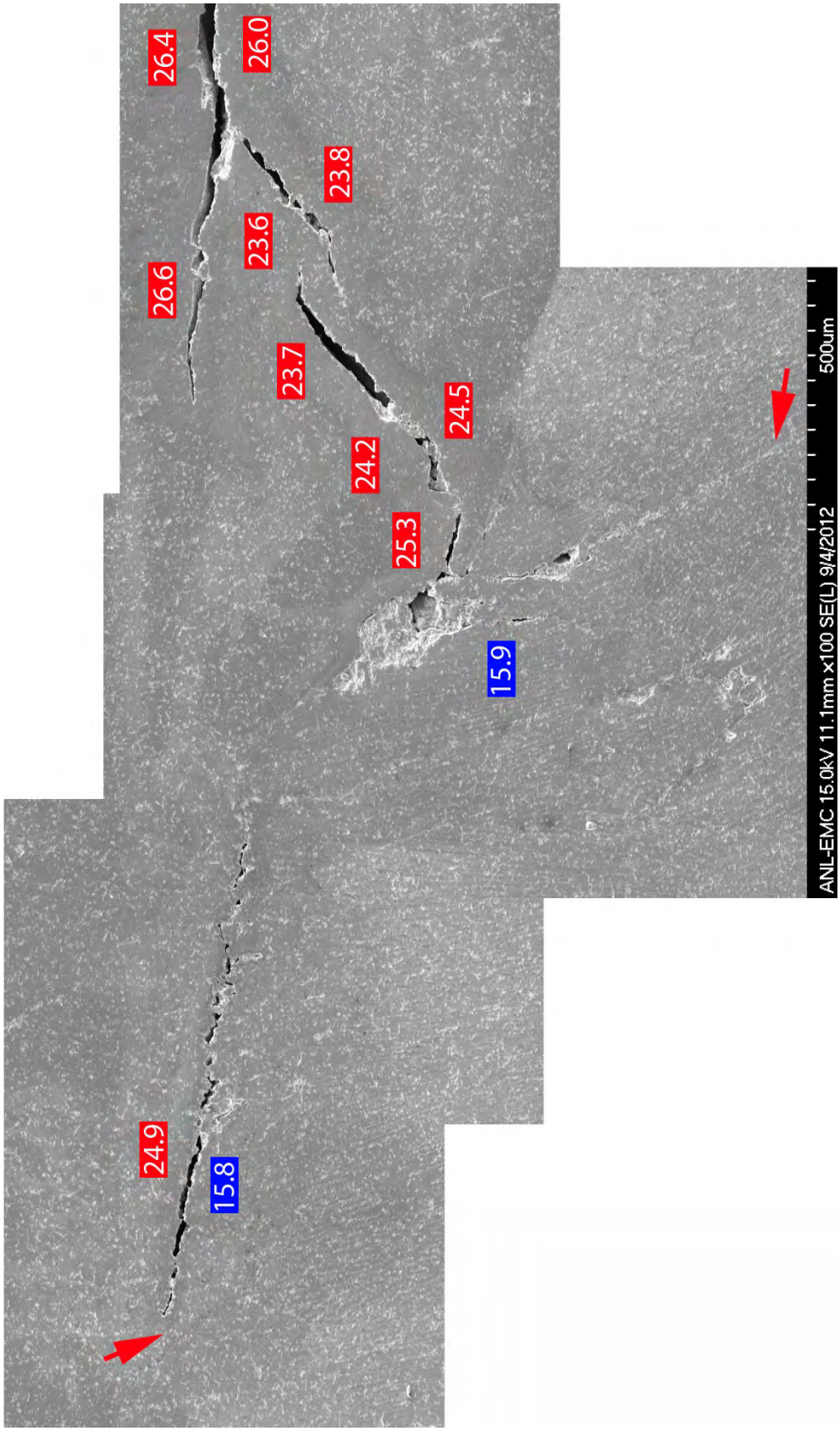

Figure 26. **Crack tip regions on the second side surface of specimen WOL-ST-2 (side M, location A in Fig. 25). Crack advance is from right to left. Cr concentration at select locations is indicated in the figure. The red arrow indicates the WOL interface.**

After the cross sections were examined, the two halves of the specimen were fractured apart after cooling in liquid nitrogen. Both appeared to have fractured along the initial direction of the crack front, i.e., along the direction labeled "1" in Fig. 25. This outcome was somewhat surprising as cracking along direction "2" (along the dendrites) seemed to feature prominently in at least two of the three cross sections examined.

The fracture surface of specimen WOL-ST-2 is shown in Fig. 27. With respect to the CT specimen geometry, the fracture surface shown corresponds to the bottom part of the specimen as shown in Fig. 17, i.e., the Alloy 182 weld is below the plane of the crack. The yellow arrows indicate the beginning of SCC growth, the red arrows show the end of the test, and the green arrows indicate the region where the crack would have intersected the interface. The relative location of each cross section (CS) described previously is indicated in the figure. Crack advance measurements on the fracture surface and the DC potential measurements are in excellent agreement (4%) for the precracking and transitioning stage. However, the crack advance under constant load was approximately 4.2 times higher than the determination by DC potential. The disparity between the DC potential and the actual measurements is not surprising given the complicated crack pattern and the large unbroken ligaments that have been observed on the cross sections. As such, a correction factor of 4.2 was applied uniformly to test periods 32-34. Table 2 and Fig. 20 already reflect that correction.

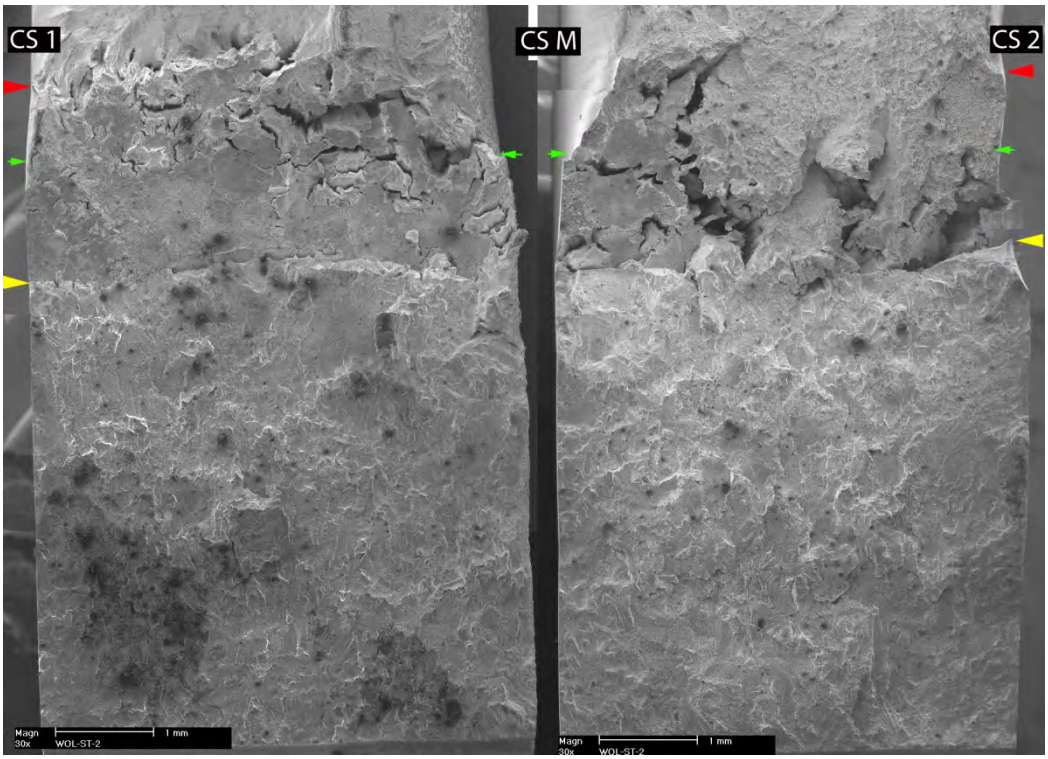

Figure 27. Fracture surface of specimen WOL-ST-2. The yellow arrows indicate the beginning of SCC growth, the red arrows show the end of the test, and the green arrows indicate the region where the crack would have intersected the interface. Crack advance is from bottom to top.

Figure 28a shows half of the fracture surface, and focuses on the region at constant load. As before, the yellow arrows indicate the beginning of SCC growth, the red arrows show the end of the test, and the green arrows indicate the region where the crack would have intersected the interface. Several locations of interest are identified in the figure. For the most part, the crack transitioned readily to an IG/interdendritic fracture mode, as observed at locations 1 and 2 (Figs. 28b, c). The morphology is consistent with an ST orientation (perpendicular to the direction of dendrites, i.e., along direction 1 in Fig.

25), and several secondary cracks can be observed. Further along, more prominent secondary cracks seem to develop, most likely along direction 2 in in Fig. 25, Figs. 28d.

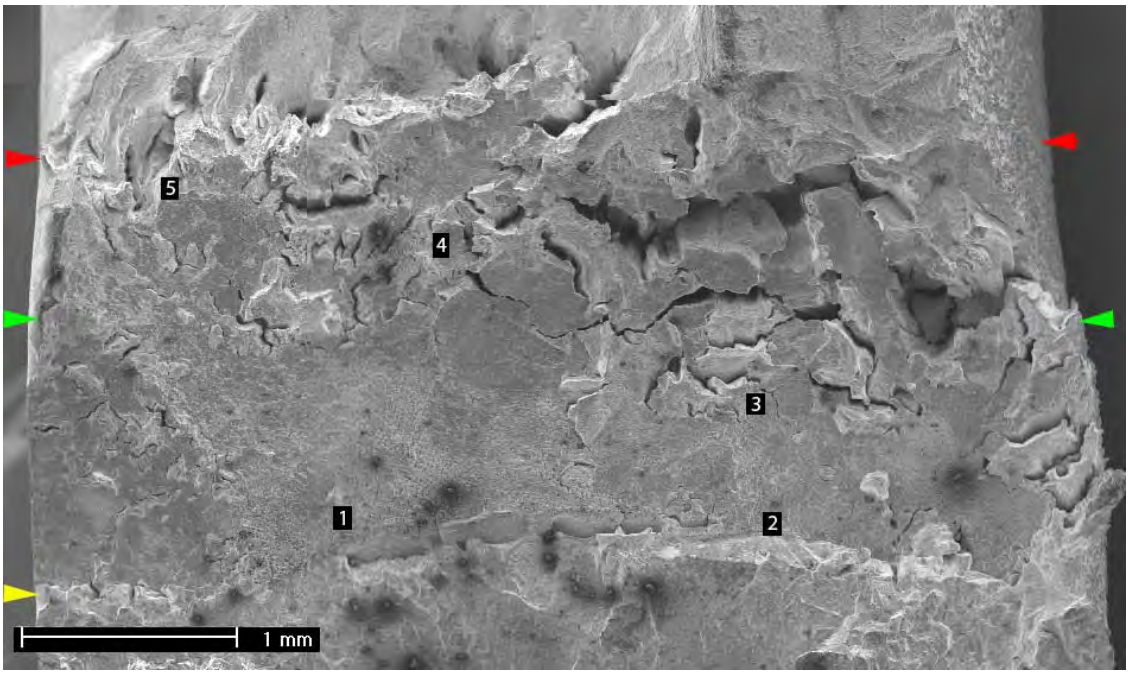

(a)

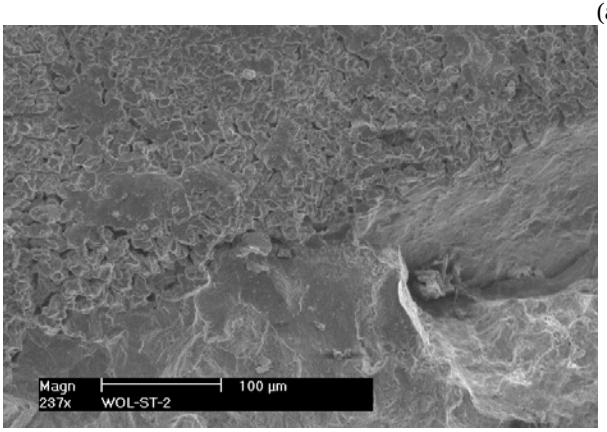

(b)

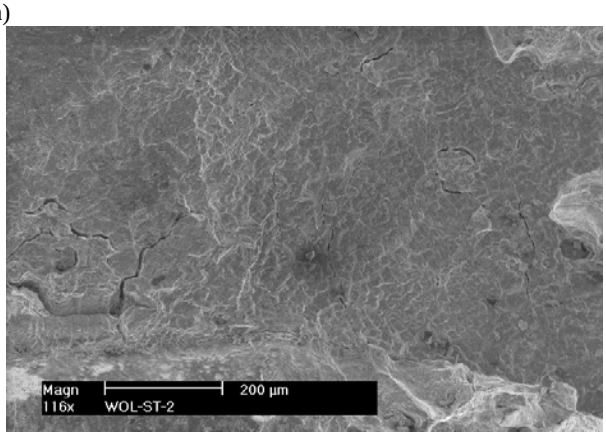

(c)

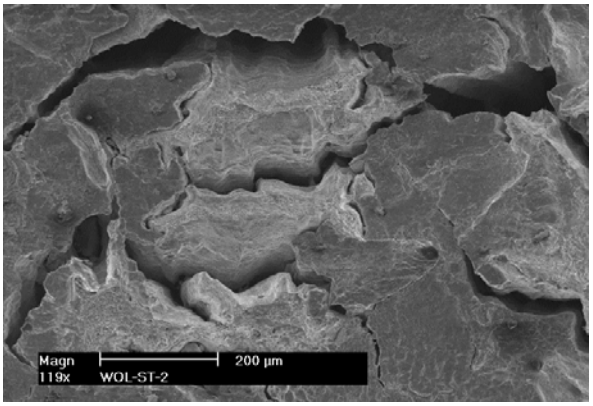

(d)

Figure 28

(a) First half (right hand side of Fig. 27) of the fracture surface of specimen WOL-ST-2 obtained under constant load in simulated primary water. (b) location 1, (c) location 2, and (d) location 3. Crack advance is from bottom to top.

Figure 29 focuses on the later part of the test. Figure 29a (location 4 in Figs. 28a) shows a combination of fracture modes: IG/interdendritic with secondary cracks, ductile rupture (white arrow) – most likely a ligament, and in the upper left hand corner, a fracture mode that seems consistent with that of the interface. Figure 29b (location 5 in Figs. 28a) shows the fracture surface at the end of the test. This exhibits an IG/interdendritic fracture mode as well as secondary IG cracks.

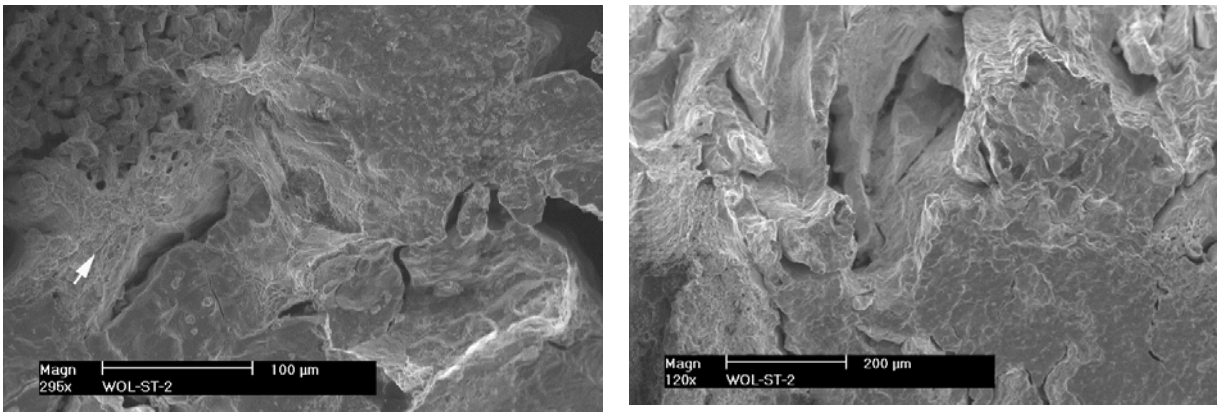

(a) (b)

Figure 29 Fracture surface of specimen WOL-ST-2 at (a) locations 4, and (b) location 5 in Fig. 28a. Crack advance is from bottom to top.

Figure 30a shows the second half of the fracture surface in the constant load region. The yellow arrows indicate the beginning of SCC growth, the red arrows show the end of the test, and the green arrows indicate the region where the crack would have intersected the interface. Several locations of interest are identified in the figure. For approximately 1/3 of the fracture surface, the appearance is similar to that shown in Fig. 28a. However, out of plane cracking - most likely along direction 2 (along the dendritic grains) in Fig. 25 - seems dominant. On this half of the specimen, cracking along the dendrites occurred early, Fig. 30b, and seems to have also been extensive. Figure 30c shows a region displaying what appears to be deep secondary cracking. Fracture morphology consistent with the weld interface (white arrow) also seems to be present.

The right hand side of Fig. 30a corresponds to the cross section shown in Fig. 24. In this particular case, the crack path was obstructed by a large ligament (Figure 24 suggested it was also off plane), but resurfaced along the weld interface. Fig. 30a provides confirmation for that initial inference, and pictures taken at location 3 provide the fracture morphology of the cracked weld interface. These images are shown in Fig. 31.

In summary the examination of the fracture surface confirmed the earlier observations on the cross sections. The crack transitioned readily to an IG/interdendritic fracture mode, and propagated in the diluted area of Alloy 52M along two main directions (labeled 1 and 2 in Fig. 25). Direction 1 (normal to the dendrites) appeared to be the dominant direction, and the secondary cracking observed on the fracture surface was mostly due to of propagation along direction 2. Upon reaching the interface, IG/interdendritic fracture mode continued.

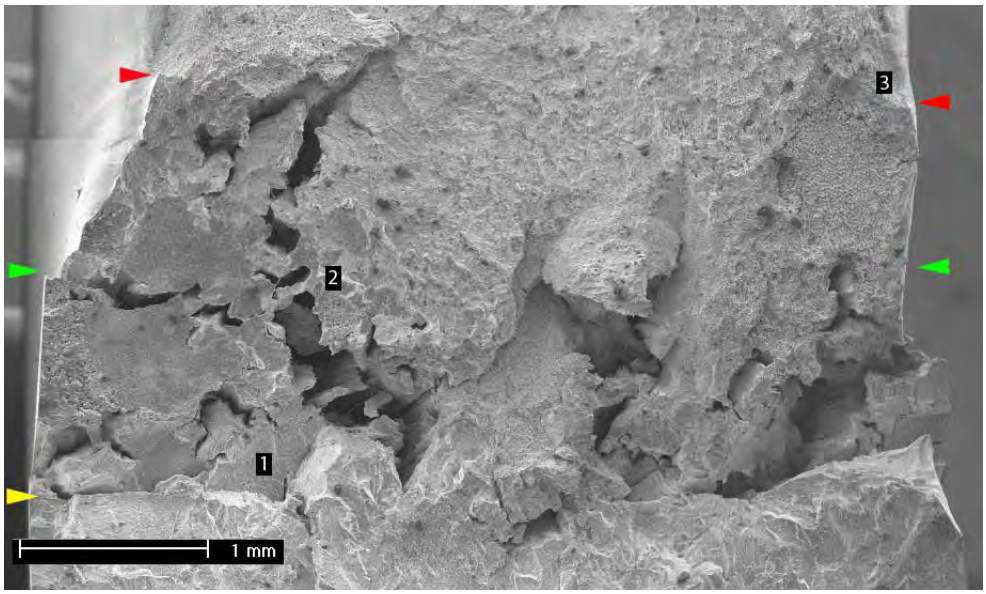

(a)

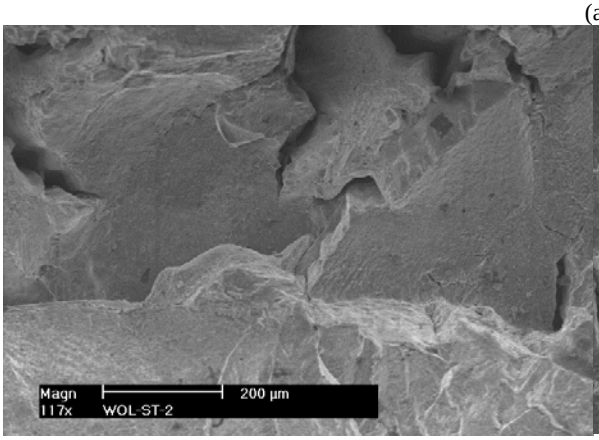

(b)

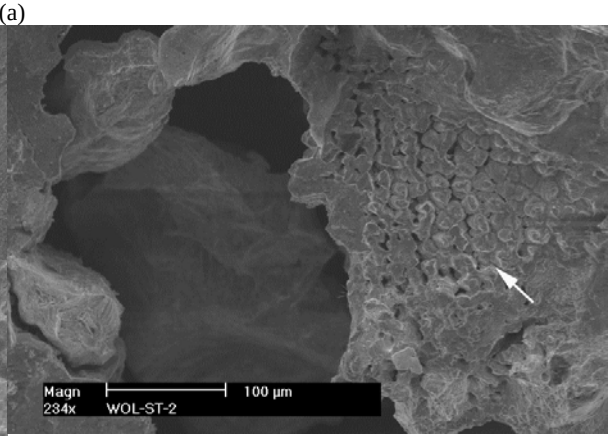

(c)

Figure 30 Second half (left hand side of Fig. 27) of the fracture surface of specimen WOL-ST-2 obtained under constant load in simulated primary water. (b) location 1, and (c) location 2. Crack advance is from bottom to top.

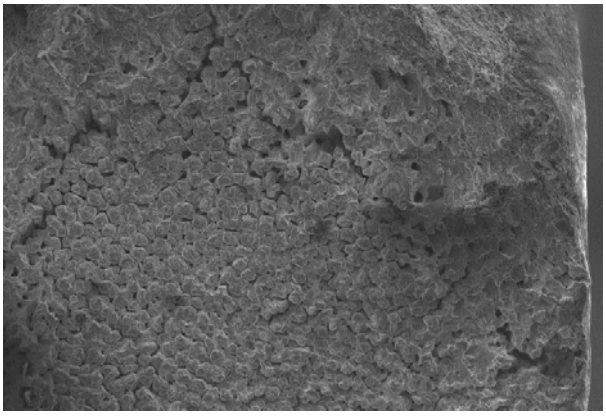

(a)

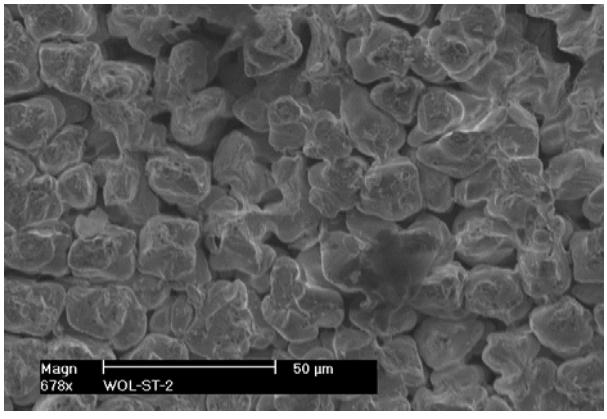

(b)

Figure 31 Fracture surface of specimen WOL-ST-2 at location 3 in Fig. 30a. Crack advance is from bottom to top.

4. DISCUSSION

SCC CGR testing on the Alloy 52M-182 WOL was conducted in two orientations: TS (earlier work[7]) and ST. Figure 32 combines the SCC CGR data obtained from these tests by illustrates these orientations and the SCC CGRs that were measured in each orientation. As described previously, the SCC CGRs in Alloy 182 are un-affected by the Alloy 52M WOL at distances larger than 1-1.5 mm from the WOL interface. However, as those cracks approached the interface in the TS orientation, the SCC CGRs in Alloy 182 were found to decrease by approx. one order of magnitude in the 1 mm leading up to the interface. The reason for the decrease is unknown, however, it may likely be due to the compressive stress exerted by the WOL. In both TS-oriented tests, significant cracking was found to develop at the interface between the two welds, and this prevented the measurement of the SCC CGR in Alloy 52M past the interface. Nevertheless, estimates based on fractography (Fig. 3) suggested that the SCC CGR in the first layer of Alloy 52M was relatively high. As such, additional testing was undertaken in the ST orientation to measure the SCC CGRs at the interface between the two welds and the first layer of Alloy 52M directly. Both the Alloy 52M-182 interface and the first layer of Alloy 52M were found to be highly susceptible. Given the long crack extensions for these measurements, and the fact that the SCC region was readily identifiable on the fracture surface, these SCC CGRs are deemed by the authors to be highly reliable.

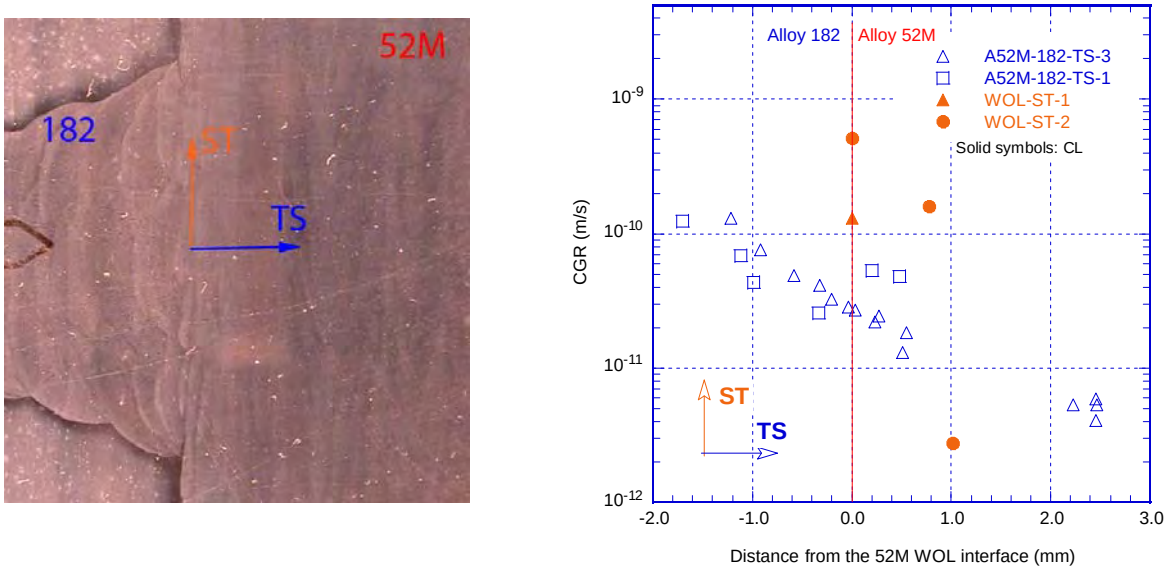

(a) (b)

Figure 32. SCC CGRs in an Alloy 52M-182 overlay: (a) Schematic showing the test specimen orientations, and (b) SCC CGRs vs. distance to the Alloy 52M-182 interface.

In order to put the Alloy 52M WOL data into perspective, Figure 33 summarizes the SCC CGR data obtained from the two ST-oriented specimens presented in this paper, along with data for Alloy 152 heat WC04F6 (28.7 wt. %) tested at ANL.[7] Also included for comparison is the MRP-115 75th percentile curve,[8] Local Cr concentrations are also included.

Figure 33 suggests that the SCC CGRs along the interface between the two welds can be as high as the MRP-115 75th percentile curve.[8] The Cr concentration for the Alloy 52M-182 interface was measured to be approx. 20 wt. %. For Alloy 52M (Fig. 33b), the Cr concentration seems to be playing a role. The SCC CGR in a region with 27.4 wt. % Cr was low, however, the unfavorable orientation of the crack vs. the dendritic grains could have played a role. However, in the first layer of Alloy 52M weld, in a region with an average Cr concentration of 25.4 wt. %, the SCC CGR was relatively high (factor 2 lower than the MRP-115 75th percentile curve[8]) despite the unfavorable orientation vs. the dendritic grains.

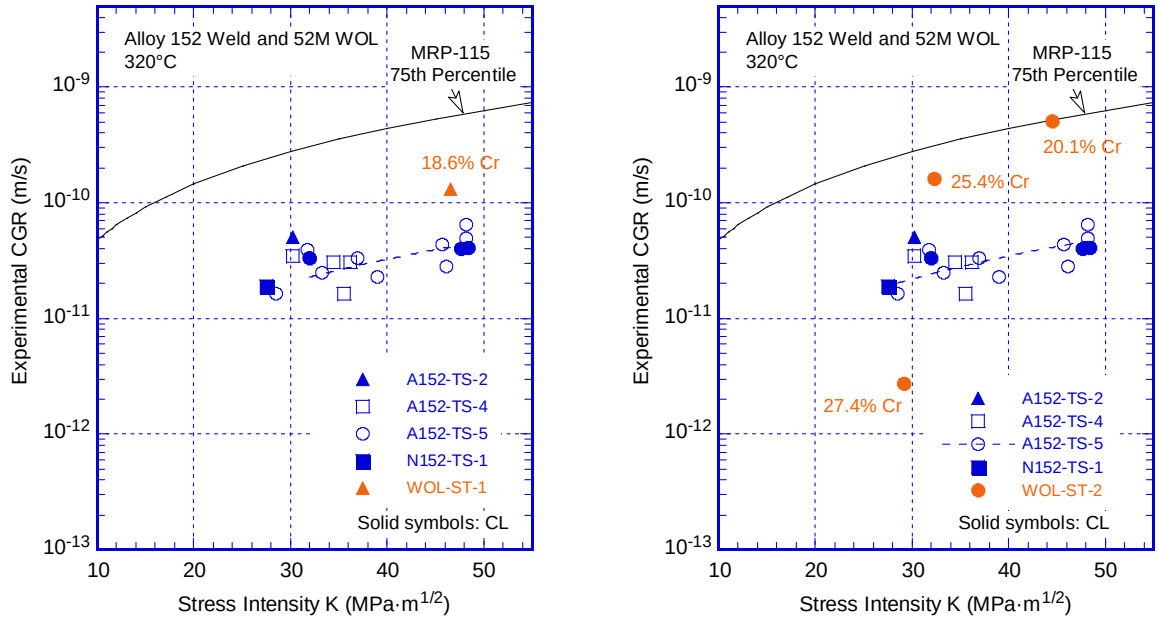

Figure 33. SCC CGRs in and Alloy 52M-182 overlay: (a) along the Alloy 52-182 interface in specimen WOL-ST-1, and (b) as a function of average Cr content in specimen WOL-ST-2. Also included are Alloy 152 data generated at ANL[7] and the MRP-115 disposition curve for Alloys 82/182.[8]

CONCLUSIONS

The SCC CGR data presented in this paper complements our prior understanding of the SCC behavior at an Alloy 52M weld overlay. In summary, SCC testing on the Alloy 52M-182 WOL was conducted in two orientations, TS and ST, and SCC CGRs were measured as a function of orientation and distance vs. the interface between the two welds. It was found that, as SCC cracks approached the interface in the TS orientation, the SCC CGRs in Alloy 182 decreased by approx. one order of magnitude in the 1 mm leading up to the interface. In both TS-oriented tests, significant cracking was found to develop at the interface between the two welds, and into the Alloy 52M WOL along the original test direction. Additional testing undertaken in the ST orientation to measure the SCC CGRs at the interface between the two welds and the first layer of Alloy 52M directly found both the interface and the first layer of Alloy 52M were found to be highly susceptible, and appear to correlate with the local concentration of Cr. The SCC CGR in the first layer of Alloy 52M weld (25.4 wt. % Cr) was a factor 2 lower than the MRP-115 75th percentile curve[8], despite the unfavorable orientation vs. the dendritic grains. The SCC CGRs along the interface between the two welds (20 wt. % Cr) was found to be as high as the MRP-115 75th percentile curve.[8]

ACKNOWLEDGEMENTS

The authors gratefully acknowledge the financial support of the U.S. Nuclear Regulatory Commission, job code V-6279. The views expressed in this paper are those of the authors, not necessarily those of the U.S. Nuclear Regulatory Commission.

REFERENCES

[1] Alexandreanu, B., Chen, Y., Natesan, K., and Shack, W. J., Cyclic and SCC Behavior of Alloy 52M/182 Weld Overlay in a PWR Environment, 15th International Conference on Environmental Degradation of Materials in Nuclear Power Systems – Water Reactors, Cheyenne Mountain Resort, Colorado Springs, Colorado, August 7-11, 2011.

[2] Alexandreanu, B., O. K. Chopra, and W. J. Shack, "Crack Growth Rates of Nickel Alloy Welds in a PWR Environment," NUREG/CR–6907, ANL–04/3, May 2006.

[3] Alexandreanu, B., O. K. Chopra, and W. J. Shack, "Crack Growth Rates of Nickel Alloys from the Davis-Besse and V. C. Summer Power Plants in a PWR Environment," NUREG/CR–6921, ANL–05/55, November 2001.

[4] PWR Materials Reliability Program Alloy 600 Issues Task Group, "Materials Reliability Program (MRP) Crack Growth Rates for Evaluating Primary Water Stress Corrosion Cracking (PWSCC) of Thick-Wall Alloy 600 Materials," MRP-55, Revision 1, Electric Power Research Institute, Palo Alto, CA, 2002.

[5] Van Der Sluys, W. A., B. A. Young, and D. Doyle, "Corrosion Fatigue Properties on Alloy 690 and some Nickel–Based Weld Metals," Assessment Methodologies for Preventing Failure: Service Experience and Environmental Considerations, PVP Vol. 410-2, ed., R. Mohan, American Society of Mechanical Engineers, New York, pp. 85–91, 2000.

[6] Psaila–Dombrowski, M. J., C. S. Wade, J. M. Sarver, W. A. Van Der Sluys, and P. E. Doherty,"Evaluation of Weld Metals 82, 152, 52, and Alloy 690 Stress Corrosion Cracking and Corrosion Fatigue Susceptibility," Proc. of the 8th Intl. Symp. on Environmental Degradation of Materials in Nuclear Power Systems-Water Reactors, S. M. Bruemmer, ed., American Nuclear Society, La Grange Park, IL, pp. 412–421, 1997.

[7] Alexandreanu, B., Chopra, O.K., Shack W.J., The Stress Corrosion Cracking Behavior of Alloys 690 and 152 Weld in a PWR Environment, 2008 ASME Pressure Vessel and Piping Division Conference, Chicago, IL, July 27-31, 2008.

[8] Materials Reliability Program: Crack Growth Rates for Evaluating Primary Water Stress Corrosion Cracking (PWSCC) of Alloy 82, 182, and 132 Welds (MRP-115), EPRI, Palo Alto, CA: 2004. 1006696.